DEFENSE DOCUMENTATION CENTER

FOR

SCIENTIFIC AND TECHNICAL INFORMATION

CAMERON STATION, ALEXANDRIA, VIRGINIA

63 - 4 - 1

TECHNICAL REPORT

PR-9

407 303

FURTHER STUDIES OF THE JET COMPRESSOR

QUARTERMASTER RESEARCH & ENGINEERING CENTER

PIONEERING RESEARCH DIVISION

MAY 1963   NATICK, MASSACHUSETTS

UNCLASSIFIED

1. Jet compressors
2. Ejectors
3. Fluid flow
4. Jets (or jet mixing)
5. Separation
6. Supersonic flow
7. Compressible flow
8. Gas flow
9. Fluid dynamic properties
I. Hoge, Harold J.
II. Segars, Ronald A.
III. Title
IV. Series

AD-   Division 9   Accession No.

Quartermaster Research and Engineering Center, Natick, Mass.
FURTHER STUDIES OF THE JET COMPRESSOR by Harold J. Hoge and
Ronald A. Segars May 1963 65 pp illus (Technical Report PR-9)

A description is given of the various regimes of flow that can exist
in the jet compressor. A new apparatus is described and data taken
with it on 6 systems of gases (He:Freon-113, He:air, air:Freon-113,
air:Freon-12, air:air, and Freon-12:air) are presented. The highest
efficiency achieved with the new apparatus is 0.125, at a compression
ratio of 1.590, with helium as the driven gas and Freon-113 as the
driving gas. Calculations of momentum-flux balance within the jet com-
pressor are made, with allowances for friction, and, when necessary,
for flow separation within the driving-gas nozzle. The changes of
available energy associated with the various processes that take place
within the jet compressor are individually calculated from the experi-
mental data. The flow rate of driven fluid is calculated as a function of
inlet pressure for the system air:Freon-113, by a method proposed by
Fabri and Siestrunck; the results represent the observations, but not
accurately.

UNCLASSIFIED

1. Jet compressors
2. Ejectors
3. Fluid flow
4. Jets (or jet mixing)
5. Separation
6. Supersonic flow
7. Compressible flow
8. Gas flow
9. Fluid dynamic properties
I. Hoge, Harold J.
II. Segars, Ronald A.
III. Title
IV. Series

FURTHER STUDIES OF THE JET COMPRESSOR

Harold J. Hoge

Ronald A. Segars

Thermodynamics Laboratory

FOREWORD

This is the latest in a series of reports and publications de-
scribing work done by the Pioneering Research Division in the field
of jet compression. The object of the program is to gain a greater
understanding of the principles of operation of the jet compressor
(ejector), in the hope that its efficiency can be increased without
the sacrifice of its present simplicity and low cost. Previous
papers have shown that the use of a heavy driving gas, such as
Freon-113, rather than a light gas, such as steam, leads to increased
efficiency.

The present paper contains experimental results obtained with a
new apparatus of different geometry. It is also a summary paper in
which our findings and conclusions are brought up to date.

One of the uses of the jet compressor is in the dehydration or
freeze-drying of foods.

                                        S. DAVID BAILEY
                                        Director
                                        Pioneering Research Division

Approved:

        DALE H. SIELING, Ph. D.
        Scientific Director

        MERRILL L. TRIBE
        Brigadier General, USA
        Commanding

i

CONTENTS

ABSTRACT

A description is given of the various regimes of flow that can exist in the jet compressor. A new apparatus is described and data taken with it on 6 systems of gases (He:Freon-113, He:air, air:Freon-113, air:Freon-12, air:air, and Freon-12:air) are presented. The highest efficiency achieved with the new apparatus is 0.125, at a compression ratio of 1.590, with helium as the driven gas and Freon-113 as the driving gas. Calculations of momentum-flux balance within the jet compressor are made, with allowances for friction, and, when necessary, for flow separation within the driving-gas nozzle. The changes of available energy associated with the various processes that take place within the jet compressor are individually calculated from the experimental data. The flow rate of driven fluid is calculated as a function of inlet pressure for the system air:Freon-113, by a method proposed by Fabri and Siestrunck; the results represent the observations, but not accurately.

FURTHER STUDIES OF THE JET COMPRESSOR

1. ## Nomenclature and Dimensions

A = cross-section area of a flow channel

A^* = cross-section area of throat of driving-fluid nozzle

B = perimeter of a flow channel

M = pertaining to the mixed regime of flow

M^* = ratio of stream velocity to velocity stream would have in choked flow

P = pressure, static or stagnation

R = gas constant

S = pertaining to the supersonic regime of flow

T = absolute temperature

W = molecular weight

a = available energy per unit mass; also, the letters a....m are used to identify the pressure taps

c^* = velocity of a stream in choked flow (sonic)

c_p = specific heat at constant pressure

f = friction factor, defined by Eq. (5)

h = enthalpy per unit mass

k = isentropic exponent

l = length of mixing tube

$\dot{m}$ = mass rate of flow

s = entropy per unit mass

u = stream velocity

x = fraction of area A_5 carrying the (separated) flow

η = efficiency of jet compressor

ρ = density of fluid

σ = shearing stress per unit area exerted by walls

ω = entrainment ratio, $\dot{m}_3/\dot{m}_1$

Superscript

* = pertaining to the sonic or choked condition

Subscripts

0 = any unspecified stagnation state

1 = initial (stagnation) state of driving fluid; also component 1, the driving fluid

2 = maximum with respect to two variables (P_8 and ω)

3 = initial (stagnation) state of driven fluid; also component 3, the driven fluid

5 = state of driving fluid as mixing begins

$5s$ = state 5 calculated isentropically from state 1

$5x$ = state 5 calculated on the assumption that a fraction x of area A_5 carries the entire flow

6 = state of driven fluid as mixing begins
7 = state of stream at completion of mixing
8 = final (stagnation) state of mixed stream
9 = state of same entropy as state 3 and same pressure as state 8
10 = state of same entropy as state 1 and same pressure as state 8
a, b, ...m = designations of pressure taps; locations are given
                    under dimensions, and are shown in Figure 7
a = based on the concept of available energy
d = pertaining to an accepted dead state
fr = pertaining to the calculation of friction loss
max = maximum value with respect to one variable (P_8)

The following dimensions refer to the apparatus used in the present experiments. A drawing of the flow channels is included in Figure 7.

Driving-fluid nozzle:

>   Width = 0.101 in.
>   length of converging part = 0.700 in.
>   length of diverging part = 0.475 in.
>   length of constant-depth part near exit = 0.100 in.
>   depth at entrance = 0.164 in.
>   depth at throat = 0.043 in.
>   depth at exit = 0.099 in.

Driven-fluid nozzle:

>   angle with mixing-tube axis = 5°
>   width = 0.206 in.
>   length of converging part = 1.100 in.
>   length of constant-depth part near exit = 0.100 in.
>   depth at entrance = 0.400 in.
>   depth at exit = 0.099 in.

Mixing tube:

>   width = 0.307 in.
>   length = 2.900 in.
>   depth = 0.099 in.

Diffuser:

>   width = 0.308 in.
>   length = 2.000 in.
>   depth at entrance = 0.099 in.
>   depth at exit = 0.400 in.

Pressure-tap locations:

Distances measured parallel to the axis of the mixing tube, from a zero plane perpendicular to the axis and passing through the end of the web that divides the driving- and driven-fluid channels. Positive direction is downstream.

$$a = -1.720 \text{ in. } (P_1)$$
$$b = -1.338 \text{ in. } (P_3)$$
$$c = -0.575 \text{ in. } (P*)$$
$$d = -0.104 \text{ in. } (P_6)$$
$$e = -0.096 \text{ in. } (P_5)$$
$$f = 0.643 \text{ in.}$$
$$g = 0.653 \text{ in.}$$
$$h = 1.393 \text{ in.}$$
$$i = 2.144 \text{ in.}$$
$$j = 2.895 \text{ in. } (P_7)$$
$$k = 3.642 \text{ in.}$$
$$l = 4.392 \text{ in.}$$
$$m = 5.142 \text{ in. } (P_8)$$

Areas:

$$A_1 = 0.0166 \text{ in.}^2$$
$$A* = 0.00434 \text{ in.}^2$$
$$A_3 = 0.0824 \text{ in.}^2$$
$$A_5 = 0.0100 \text{ in.}^2$$
$$A_6 = 0.0204 \text{ in.}^2$$
$$A_7 = 0.0304 \text{ in.}^2 \ (=A_5 + A_6)$$
$$A_8 = 0.1232 \text{ in.}^2$$

Area ratios:

$$A_1/A* = 3.82$$
$$A_5/A* = 2.30$$
$$A_3/A_6 = 4.04$$
$$A_6/A_5 = 2.04$$
$$A_8/A_7 = 4.05$$

2. Introduction

The jet compressor (ejector) has been an object of study for many years, yet it is easy to find diverging opinions and conflicting recommendations on how to build a good ejector. Within the past decade an understanding of the various flow patterns that can exist within a jet compressor has developed. These flow patterns, and the transitions between them, account qualitatively for the observed behavior of ejectors.

Quantitative calculations, based on the equations of energy, continuity, and momentum-flux can be made for jet compressors. Such calculations are helpful in understanding the flow patterns and in verifying assumptions that have been made. However, for a jet compressor of given geometry such calculations do not fully specify the operating state in terms of the input stagnation conditions, since they permit a multiplicity of solutions.

Further progress in understanding the ejector will require empirical or theoretical attacks that involve the mixing process itself in some way, rather than the states immediately before and immediately after mixing. A few attempts in this direction have been made, but quantitative experimental confirmations of assumed mixing mechanisms are still scarce.

A number of laboratories, including our own, have set out to methodically study the various factors that influence jet-compressor performance. Our own previous experimental work (1, 2) has shown the results of maximizing the efficiency of an ejector with respect to variations in outlet pressure, entrainment ratio, and the nature of the driving and driven gases. These results refer to a single ejector and cast no light on what may happen when the geometry of the compressor is changed.

The present paper extends the study to an apparatus of different geometry. It begins with a general description of the flow in an ejector, without any systematic attempt to show the experimental proof of existence of the various regimes of flow. This is followed by a presentation of the new experimental work done since our last reports. Next, the picture of the compression process presented at the beginning is examined in a number of quantitative calculations, using principally our own data but in one case those of other observers. A few peculiar and unexplained phenomena are discussed. Finally, a proposed method of calculating the supersonic regime is tried out, and the present state of our knowledge is summed up.

3. Nature of the Flow in a Jet Compressor

In a jet compressor (ejector) two streams of fluid are accelerated; they are brought into contact with each other so that they mix, come to the same pressure and usually to approximately the same velocity and temperature, and finally the mixture is brought to rest. The driving stream experiences a net fall in pressure, and the driven stream experiences a net rise in pressure. The ejector is a device for doing useful work by compressing the stream of driven fluid. It can serve as an ordinary compressor, as a vacuum pump, or as a machine for circulating air or other gases.

Figure 1 contains a schematic diagram of a jet compressor, and three partial diagrams. Each diagram shows a different regime or pattern of flow. These patterns of flow have been identified and described by Fabri and Siestrunck (3), using ideas presented earlier by Fabri, Le Grivès, and Siestrunck (4). A paper by Fortini (5) contains a good presentation of several of the basic ideas, and others have used them. Among the things still lacking is a knowledge of detailed mechanisms. For example, when does one regime yield to another? When the input and output pressures are given, what mechanism determines the mass rate of flow of driven fluid?

The ejector shown schematically in Fig. 1 has a converging-diverging nozzle for the driving fluid, which we assume to be a gas. This gas has a stagnation pressure P_1, a stagnation temperature T_1, and a mass-flow rate $\dot{m}_1$. Driving gas enters the mixing tube through the nozzle-exit-plane 5 at supersonic speed. Driven gas enters the ejector through a converging channel. Its stagnation pressure is P_3, its stagnation temperature is T_3, and its mass rate of flow is $\dot{m}_3$. (The nomenclature adopted here is given in Section 1. It agrees with that used in references (1) and (2), with minor changes.) The driven gas enters the mixing tube through the plane 6, which is shown as an annular area surrounding the driving-gas nozzle. Usually, the entering flow is subsonic, but if the stagnation pressure P_3 of the stream is made high enough, sonic flow may exist in plane 6. The subscripts, 5, 6, etc., will be used to distinguish any variables referring to the gas or the channel at the corresponding point in the channel. Thus, for example, the plane 5 has an area A_5, and the pressure of the gas passing through it is P_5.

The ejector shown in Fig. 1 has constant-area mixing. The mixing tube has throughout its length a constant area equal to its exit area A_7,

Mixing Tube

Diffuser

$P_1, T_1, \dot{m}_1$

$P_3, T_3, \dot{m}_3$

6

5

6

7

8

Supersonic Regime

Mixed Regime

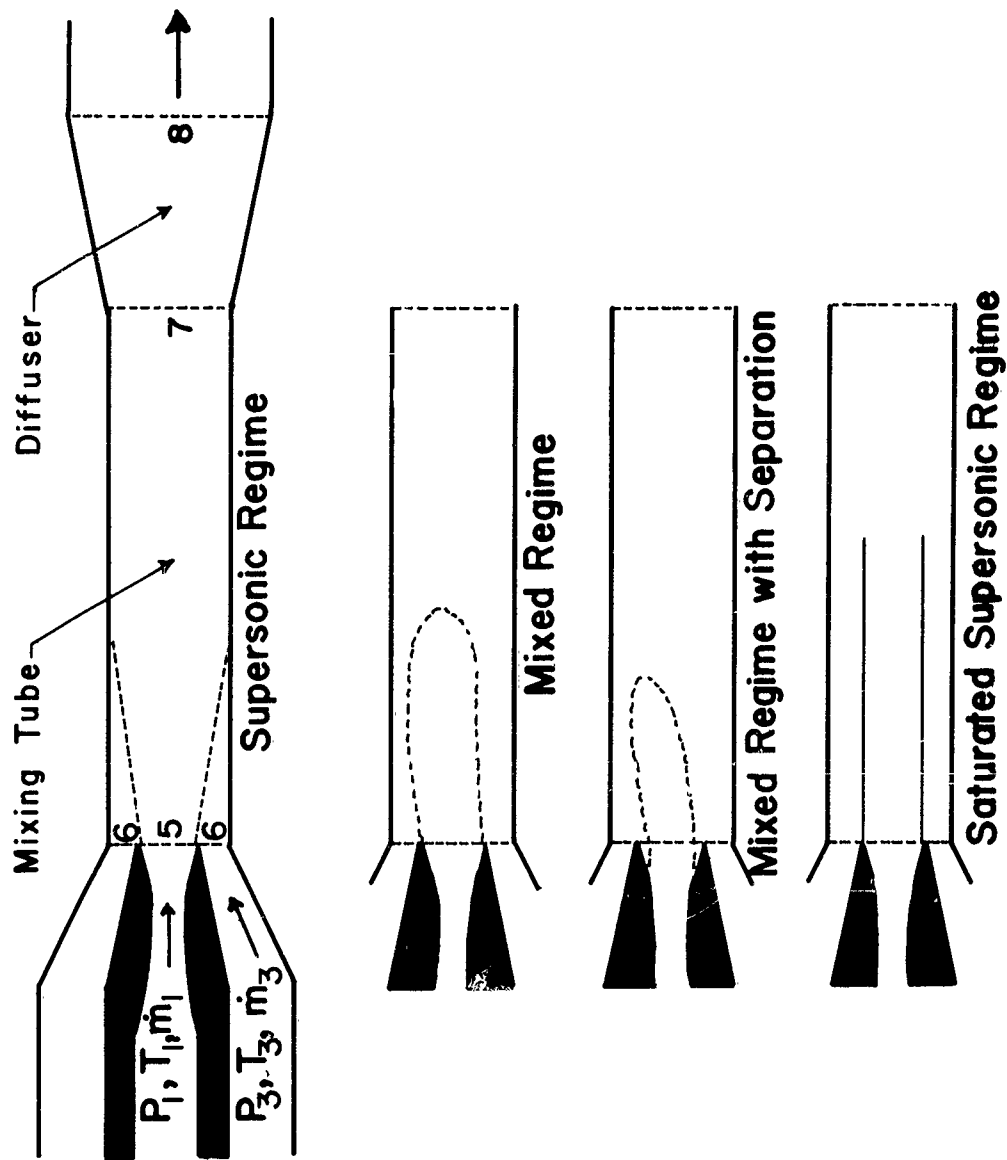**Mixed Regime with Separation**

Saturated Supersonic Regime

Fig. 1. Schematic diagram of a jet compressor, with illustrations of the four different regimes of flow.

and the areas of the two streams at the entrance satisfy the relation A_5 + A_6 = A_7. Constant-area mixing is particularly simple from the mathematical standpoint.

The length of a mixing tube is generally 8 to 10 times its diameter. In this length enough mixing takes place to give good operating characteristics, and wall friction is held to reasonable limits.

The section of the ejector between planes 7 and 8 is the diffuser, in which the mixed stream is decelerated and its pressure is raised. Normally, the flow entering the diffuser is subsonic. If this flow is supersonic, the efficiency of the jet compressor will be low. There is some indication, however, that it is desirable for the flow to enter the diffuser at a velocity only slightly below sonic.

When the flow of driven fluid ($\dot{m}_3$) is zero, the area A_6 carries no net flow and could be closed off by a solid surface without affecting the flow of driving fluid. The jet compressor is then equivalent to a flow channel in which there is a sudden enlargement. There is considerable literature on the flow at a sudden enlargement, and since the problem is a limiting case of the ejector problem it is worthwhile to treat the two problems together. Note that a laboratory vacuum pump operating on a closed system may approach the sudden-enlargement conditions quite closely.

The Supersonic Regime. A jet compressor is usually operated in the supersonic regime. This regime or flow pattern is illustrated in the upper diagram of Fig. 1. The supersonic regime exists when any cross section of the mixing tube is completely filled with supersonic flow. There is of course always a region of subsonic flow in the boundary layer at the walls of the mixing tube, but in the supersonic regime this layer is thin. The effect of downstream conditions cannot be propagated upstream through the supersonic flow; hence the upstream flow pattern is substantially independent of downstream conditions.

In Fig. 1 the dashed lines extending from the exit of the driving-fluid nozzle to the walls of the mixing tube indicate schematically the boundary between supersonic and subsonic flow. The entrance pressure P_5 of the driving fluid is usually somewhat higher than the entrance pressure P_6 of the driven fluid. The stream of driving fluid therefore continues to expand after it leaves the nozzle and the channel

7

available for the subsonic driven stream converges. Because of this convergence, the driven stream must accelerate within the mixing tube. The interaction of the driving and the driven stream also accelerates the latter, so that finally all of the driven stream except the unavoidable boundary layer reaches or exceeds sonic velocity.

The ends of the diverging dashed lines indicate the first cross section at which the entire mixing tube is filled with attached supersonic flow. Downstream from this cross section, mixing continues and velocity as a function of mixing-tube radius undoubtedly becomes more uniform. In the downstream portion of the mixing tube there is normally an extended shock, in which the supersonic flow is converted to subsonic flow.

The supersonic regime is obtained when the expansion ratio, P_1/P_8, is relatively large. The exact value required by a given ejector depends on its geometry and also on the mass rate of flow of driven fluid $\overset{\circ}{m}_3$. It is useful to determine experimentally the value of P_1/P_8 required to establish the supersonic regime when $\overset{\circ}{m}_3$ is zero. If then $\overset{\bullet}{m}_3$ is made greater than zero, P_1/P_8 also will have to be increased, if the supersonic regime is to be maintained. When a jet compressor is operating in the supersonic regime, increase in P_8 or decrease in P_1 will eventually cause the flow pattern to change, with the supersonic regime giving place to the mixed regime.

Before proceeding to discuss the mixed regime, a few qualifying remarks will be made about the supersonic flow that (we have postulated) must fill the entire mixing tube except for a thin boundary layer. The assumption of supersonic flow over the entire cross section comes from the observed fact that downstream changes do not affect upstream flow. Pearson, Holliday, and Smith (6) have shown that there is a generalized form of choked flow, in which downstream changes are not propagated upstream through the plane of choking, and yet the flow consists of two unmixed streams side by side, one supersonic, the other subsonic by conventional standards. In very general terms, the supersonic nature of one stream compensates for the subsonic nature of the other stream, with the result that the plane of choking has a sonic nature, and no pressure pulse can be propagated upstream through it.

The experimental results of Pearson, Holliday, and Smith were obtained in very short mixing tubes (shrouds at the exit of a jet engine)

and it is not clear whether or not similar conditions exist in a conventional ejector. We will qualify the statements made in earlier paragraphs by saying that any mechanism that produces a plane or region that isolates the upstream flow from changes in downstream conditions is adequate to establish the supersonic regime.

The Mixed Regime. The mixed regime of flow occurs in a jet compressor when the ratio P_1/P_8 is not large enough to sustain the supersonic regime. An ejector operating in the supersonic regime will go over into the mixed regime as P_1 is lowered or P_8 is raised. The transition may be detected by the large readjustments in pressure that occur as P_8 is changed. Changes are especially noticeable in P_3 and P_6. References to "pickup" and "break" occur in the literature. "Pickup" probably refers to transition from the mixed to the supersonic regime, and "break" to transition in the opposite direction.

The mixed regime is illustrated in the second diagram of Fig. 1. The exit of the driving-fluid nozzle is completely filled with supersonic flow, but this flow does not completely fill the mixing tube. Supersonic flow is limited to a space such as that bounded by the dashed line. Inside this region a shock pattern exists, through which the supersonic flow is rapidly converted to subsonic. The axis of the supersonic core does not necessarily coincide with the axis of the mixing tube, but may go off at an angle, as shown in the figure.

A subsonic path of pressure communication exists between the downstream and the upstream ends of the mixing tube. If the outlet pressure P_8 is raised, the pressures P_6 and P_3 rise with it.

The Mixed Regime with Separation. High values of the expansion ratio P_1/P_8 produce the supersonic regime. Lower values give the mixed regime in which the flow in the mixing tube has changed but the flow within the diverging portion of the driving-fluid nozzle remains supersonic. At still lower values of P_1/P_8 the pressure of the subsonic gas surrounding the supersonic flow is large enough to cause separation of the flow within the driving-fluid nozzle. This gives the mixed regime with separation, which is illustrated in the third diagram of Fig. 1.

The plane of separation moves upstream as P_1/P_8 is decreased. Separation of the flow is almost always accomplished through an oblique-shock pattern. A single normal shock would appear to be possible but is

9

seldom observed. A core of separated supersonic flow persists down-stream from the plane of separation, as shown by the dashed line, but is soon converted to subsonic flow.

The Saturated Supersonic Regime. In the supersonic regime, the driving fluid enters the mixing tube at supersonic speed and the driven fluid enters at subsonic speed. At a given stagnation pressure P_3 of the driven fluid, the process that determines the mass rate of flow of driven fluid $(\dot{m}_3)$ is the interaction between the driving and driven streams within the mixing tube. If the pressure P_3 is raised, the flow of driven fluid in the entrance plane will become sonic, and the flow will then be limited by choking in this plane rather than by interaction between the two streams. This situation gives the saturated supersonic regime, which is illustrated in the bottom diagram of Fig. 1.

In the saturated supersonic regime there appears to be very little change in the cross sections of the two streams as they flow through the mixing tube. Since plane A_6 is a throat, the driven stream cannot converge within the mixing tube. Divergence is permissible, but this would require P_6 to be greater than P_5 and separation might occur within the driving-fluid nozzle.

In the experiments now being reported the saturated supersonic regime was not observed. The three other regimes described above were all observed. It seems likely that the ratio A_6/A_5 in our apparatus was too large for the saturated supersonic regime to be conveniently accessible.

The paper by Fabri and Siestrunck (3) contains shadowgrams of actual flow patterns illustrating the four regimes of flow in ejectors.

4. Experimental Measurements

The present study contains results for six systems, as follows (the driven gas is given first): He:Freon-113, He:air, air:Freon-113, air:Freon-12, air:air, and Freon-12:air. For brevity, a specimen run has been selected for detailed presentation, and the rest of the results have been given in less detail. The run selected (run 45, air:Freon-113) is a typical one and exhibits most of the phenomena of interest.

10

One of the requirements laid down for the present experiments was that it should be possible to measure the pressures of the driving and driven streams at several points before they mixed, and at the cross section where mixing began. In addition, it was desired to measure pressures at several points along the length of the mixing tube and the diffuser. These requirements were met by adopting a new design for the apparatus. Our first apparatus had the conventional axial symmetry, with channel cross sections that were either circles or annuli; hence no measurement of pressure could be made on the driving stream after it entered the nozzle. In the new apparatus the flow channels are of rectangular cross section. These channels were milled in the flat surface of a brass bar, and when the apparatus is assembled these channels are covered by a flat, gas-tight lid in which the pressure taps are mounted.

Apparatus. Figure 2 is a photograph of the assembled apparatus. The flat bar containing the flow channels is clamped between two brass plates, one of which carries the pressure taps. Two inlet tubes of intermediate size and a large outlet tube are mounted in the same plate that carries the pressure taps. A scale drawing of the flat bar containing the flow channels is given in section 6 of this paper, as part of Fig. 7. The locations of the 13 pressure taps are shown by the small dots in the figure, and their distances from the cross section where the entering streams merge are given in section 1 (Nomenclature and Dimensions). The letters a, b,...m beside the pressure taps are used to identify readings when data are being recorded.

The necessary variation in cross section of the various flow channels is obtained by varying the depth of each channel appropriately. The top and sides of each channel are plane surfaces, but the depth of each channel is changed as necessary to obtain the desired convergence or divergence. The depths as functions of distance along the direction of flow are specified by cubic equations. Four equations were required: one for the subsonic part of the driving-fluid nozzle, one for the supersonic part, one for the driven-fluid nozzle, and one for the diffuser. The driven-fluid nozzle was entirely converging and the diffuser was entirely diverging. The cubic contours each had zero slopes at the two ends and a point of inflection at the midpoint. Each was symmetrical about its midpoint. It was thought that these cubic contours would be somewhat superior to simple ramp functions, and that more elaborate channel shapes calculated by the method of characteristics were hardly justified.

11

Fig. 2. Photograph of the apparatus.

The channels were cut with a milling machine, using a cutter-wheel of known diameter and a width equal to the desired width of the channel. The machinist cut each channel with the aid of a table of x,y settings specifying successive, closely-spaced positions of the milling-machine table. Allowance was made for the fact that, because of the finite diameter of the cutter, the shape of the channel is not an exact duplicate of the path of the work relative to the cutting-wheel axis. After the channels were cut they were measured with a depth gage and enlarged graphs plotted on coordinate-ruled tracing paper. The graphs were superposed on graphs of the desired curves and showed adequately good agreement.

The apparatus gives constant-area mixing. That is, the cross-section area of the mixing tube is equal to the sum of the cross-section areas of the driving and driven streams at the point where mixing begins. Constant-area mixing was adopted principally because it is easier to treat theoretically than other situations.

. The flat bar containing the flow channels can be moved longitudinally relative to the plates between which it is clamped. Hence the positions of the pressure taps relative to the flow channels are not fixed but may be moved up or down stream. The positions of the taps given in section 1 were chosen because they placed tap c directly over the throat of the driving-fluid nozzle. Note that taps d and e, with which the pressures at the beginning of mixing are measured, are slightly upstream from the end of the web that separates the driving and the driven streams. This was unintentional; the web was longer than expected. The channel depths do not change downstream from taps d and e, and the pressures observed at these taps are believed to be quite close to the actual mixing pressures.

· In some preliminary measurements, sets of pressure readings were made at a series of bar positions, with care taken to duplicate the conditions of flow as accurately as possible each time the apparatus was reassembled after moving the bar. The bar was moved 1/8 inch longitudinally each time, until the observations covered the entire length of the mixing tube at 1/8-inch intervals. This detailed exploration of pressure distribution was time-consuming, and did not add greatly to the information obtained from a single set of readings. Hence the bar was positioned as described above and not moved during the reported measurements.

13

Pressures were measured as in our previous work (1) with an absolute mercury manometer to measure the higher pressures and an oil manometer to measure certain pressure differences with high accuracy. All pressures are reported in mm Hg absolute. Oil-column heights were converted to equivalent mercury heights with the experimentally-determined density ratio.

Measurement of flow rates was by means of the same dry gas meters that were used in the previous work, except in one case. Freon-113 cannot be passed through a dry gas meter at room temperature because its vapor pressure is less than 1 atmosphere and the higher external pressure would cause the meter to collapse. Freon-113 was used only as a driving fluid, and was metered by the driving-fluid nozzle. The flow rates were adjusted by means of needle valves. The outlet pressure was subatmospheric, maintained by a large vacuum pump of 15 cfm capacity.

Procedure. The procedures described in reference (1) were followed. The flow rates were first set to the desired values. Then the outlet pressure P_8 was lowered until the compression ratio P_8/P_3 was near unity, and a set of pressure measurements was made. Such a set of measurements we refer to as an experimental point. After each point, the value of P_8 was increased and the process repeated. A run consisted of from 10 to 25 points, at increasing values of P_8, made without changing the flow rates.

Compression ratios P_8/P_3 were computed and plotted as each run progressed, so that the measurements would be suitably spaced and so that all regions of interest would be covered. The two flow rates $\dot{m}_1$ and $\dot{m}_3$ were measured at the beginning and end of each run, and at as many intermediate times as conditions required. The entrainment ratio ω, which is the ratio of the flow rates of driven and driving fluids $(\dot{m}_3/\dot{m}_1)$, ordinarily remained constant within 1 per cent or better during a single run. Between one run and another, $\dot{m}_1$ was normally held at the same value and $\dot{m}_3$ was changed.

Effect of Varying the Outlet Pressure, and Calculation of Efficiency. As the outlet pressure P_8 is increased, the entrainment ratio being held constant, the compression ratio first rises, then falls. Under certain conditions it may rise again to a second maximum and fall again as P_8 is increased. Figure 3 shows the compression ratio P_8/P_3 plotted against outlet pressure, for 8 runs made on the system air:Freon-113. The entrainment ratio for each run is indicated beside it on the graph.
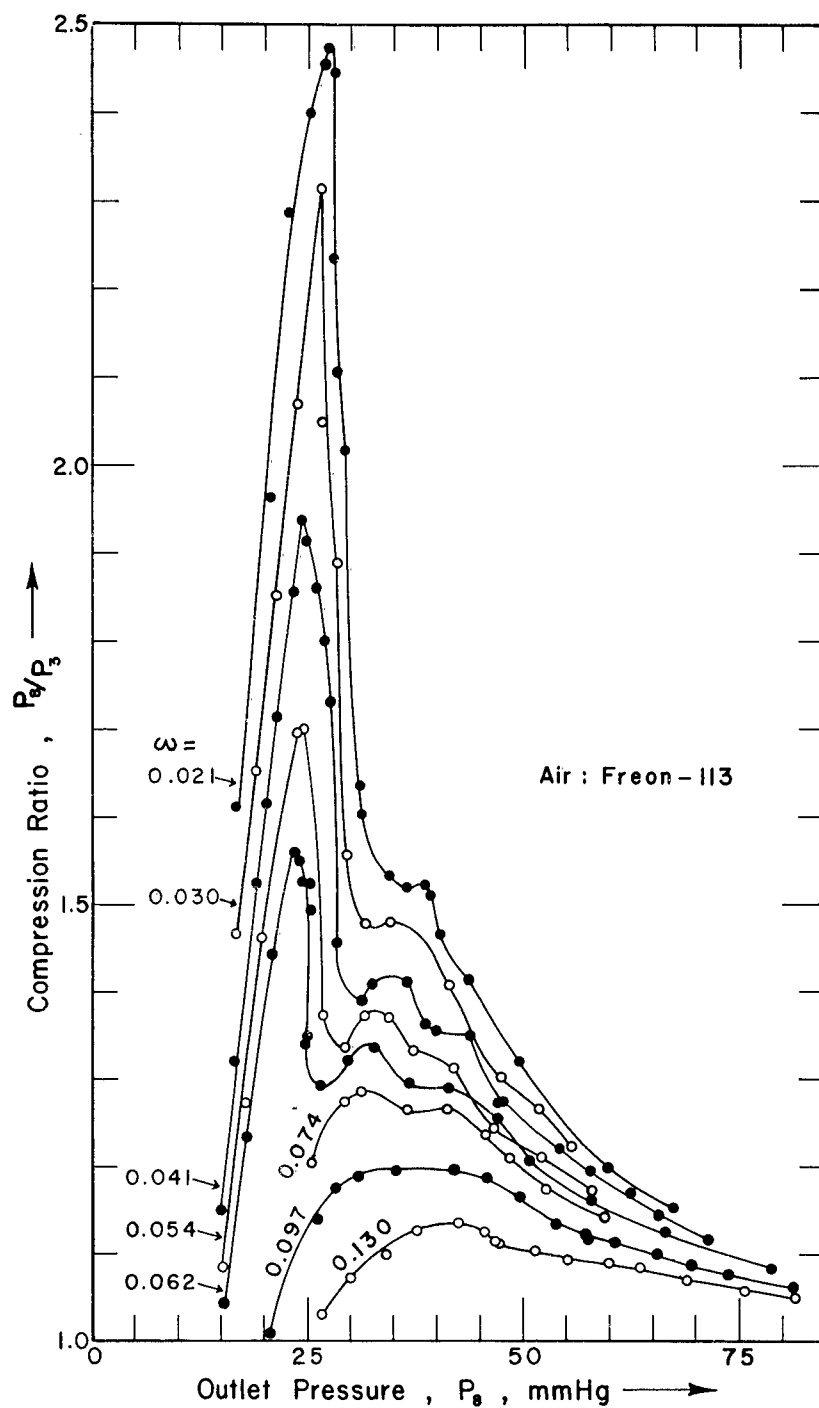
Fig. 3. Compression ratio P_8/P_3 versus outlet pressure P_8
for 8 selected runs on the system air:Freon-113.
Runs 36, 39, 40, 42, 44, 45, 51, 55 are shown. To
identify runs, find ω-values in Table 2c.

15

The specimen run 45, which has been selected for complete presentation, is included in the group. It may be identified by its entrainment ratio, which was 0.041. There were 9 additional runs made on the system air:Freon-113 (17 in all). These runs were of course plotted when the data were being analyzed, but have been omitted from Fig. 3 to avoid confusion.

Numerical data for the specimen run (Run 45) are given in Table 1, parts a and b. This run consisted of 25 points (sets of pressure measurements) designated 45.1, 45.2... 45.25, the number following the decimal point indicating rank in order of increasing P_8. Seven of the 25 points (as indicated in the column headings) are included in Table 1. All 25 points are shown in Fig. 3.

All data for all the systems studied were plotted as in Fig. 3. The next step, also carried out for all data, was to compute the efficiency of the compression process. The formula for efficiency was derived in reference (1). It is

$$\eta = \omega \frac{h_9 - h_3}{h_1 - h_{10}} \tag{1}$$

wherein η is efficiency, $h_9 - h_3$ is the isentropic enthalpy rise of unit mass of driven fluid between its initial state 3 and the outlet pressure P_8, and $h_1 - h_{10}$ is the isentropic enthalpy drop of unit mass of driving fluid between its initial state 1 and the outlet pressure P_8. This form of the efficiency equation was used in the early part of the present work. Enthalpies were taken from various tabulations, particularly from the Gas Tables of Keenan and Kaye (7).

While the measurements were being made, it became possible to calculate the data on an IBM-650 computer. Since the use of tables is relatively much more difficult for a machine than for a human computer, Eq. (1) is not well suited for machine computations. The use of tabulated enthalpies was therefore given up and enthalpies were expressed in the form of equations. If c_p, the heat capacity of a gas at constant pressure, is constant, its enthalpy is given by

$$h - h_0 = c_p (T - T_0) \quad .$$

16

where the subscript zero refers to some reference state such as the stagnation state. Along an isentrope

$$T/T_O = (P/P_O)^{\frac{k-1}{k}}$$

where k is cp/cv, the ratio of the specific heats at constant pressure and at constant volume. Using these relations, Eq. (1) may be written

$$\eta = \omega \; \frac{c_{p_3} T_3}{c_{p_1} T_1} \; \frac{\left(\frac{P_8}{P_3}\right)^{\frac{k_3-1}{k_3}} - 1}{1 - \left(\frac{P_8}{P_1}\right)^{\frac{k_1-1}{k_1}}} \tag{2}$$

where T_3 is the stagnation temperature of the driven stream, T_1 the stagnation temperature of the driving stream; c_{p_3} and k_3 refer to the driven stream, and c_{p_1} and k_1 refer to the driving stream.

Equation (2) was used instead of Eq. (1) in the machine computations. All specific heats and k-values were treated as constants. A few sets of observations were computed both with Eq. (1) and with Eq. (2), and the differences were found to be negligible for our purposes.

Figure 4 shows efficiency as a function of outlet pressure, for 4 of the runs shown in Fig. 3. The efficiency curves are somewhat distorted reproductions of the corresponding compression-ratio curves. It is clear from Eq. (2) that this should be expected. The numerator follows the variation in P_8/P_3. The denominator decreases somewhat as P_8/P_1 increases. The result is that η follows the variations in P_8/P_3 but with η rising relatively higher than P_8/P_3 at high values of P_8.

In Fig. 4 many of the curves cross each other, and they tend to pile up at low values of P_8. For this reason only 4 of the 8 curves of Fig. 3 are included in Fig. 4. Three of the four curves in Fig. 4

TABLE 1. DATA FOR RUN 45. This run is the specimen run for which data and computations are presented much more completely than for any of the other runs. System: air:Freon-113.

Point →	45.1	45.5	45.9	45.13	45.17	45.21	45.25
a. Flow rates, pressure ratios, efficiencies, etc.							
$\dot{m}_1$, lbm hr^{-1}	2.474	2.474	2.482	2.474	2.482	2.474	2.467
$\dot{m}_3$, lbm hr^{-1}	0.104	0.103	0.103	0.102	0.101	0.100	0.100
$\dot{m}_7 = \dot{m}_1 + \dot{m}_3$	2.578	2.577	2.585	2.576	2.583	2.574	2.567
$\omega = \dot{m}_3/\dot{m}_1$	0.0421	0.0417	0.0413	0.0412	0.0408	0.0406	0.0404
P_8/P_3 = compression ratio	1.150	1.716	1.860	1.389	1.356	1.220	1.117
P_8/P_1 = expansion ratio	0.098	0.141	0.171	0.206	0.262	0.357	0.472
P_6/P_5 = mixing-pressure ratio	0.659	0.649	0.738	1.144	1.157	1.262	1.184
P_5/P_1	0.125	0.122	0.121	0.128	0.166	0.231	0.356
η = ordinary efficiency	0.0182	0.0862	0.1093	0.0615	0.0659	0.0540	0.0402
η_a = efficiency based on availability	0.016	0.074	0.094	0.055	0.060	0.051	0.039
b. Pressures, mm Hg							
Tap a (P_1)	152.0	152.0	152.5	152.0	152.5	152.0	151.5
b (P_3)	13.0	12.5	14.0	22.5	29.5	44.5	64.0
c (P^*)	90.5	90.5	90.5	90.5	90.5	90.5	90.0
d (P_6)	12.51	12.04	13.58	22.24	29.30	44.37	63.93
e (P_5)	18.99	18.55	18.39	19.44	25.33	35.16	53.97
f	9.39	8.89	13.80	22.21	29.30	43.95	63.74
g	9.06	8.59	12.27	22.34	29.70	44.14	63.97
h	10.33	9.86	17.74	22.89	30.64	46.03	66.21
i	10.72	11.36	21.26	25.01	33.47	49.45	69.37
j (P_7)	12.45	17.77	22.56	27.35	36.66	52.12	70.18
k	11.63	19.66	24.29	28.94	38.45	53.45	71.00
l	14.07	20.60	25.33	30.34	39.59	54.10	71.39
m (P_8)	14.95	21.45	26.04	31.26	40.01	54.27	71.49

TABLE 1 (Continued)

Point →	45.1	45.5	45.9	45.13	45.17	45.21	45.25
			c. Momentum-flux balance				
u_5, $Btu^{\frac{1}{2}}$ $lbm^{-\frac{1}{2}}$	4.50	4.58	4.62	4.42	3.57	2.66	1.78
u_6, $Btu^{\frac{1}{2}}$ $lbm^{-\frac{1}{2}}$	1.04	1.08	0.95	0.58	0.44	0.28	0.20
u_7, $Btu^{\frac{1}{2}}$ $lbm^{-\frac{1}{2}}$	3.09	2.23	1.78	1.48	1.11	0.78	0.58
$\dot{m}_1 u_5 + P_5 A_5$	13.82	13.96	14.08	13.69	12.45	11.57	12.02
$\dot{m}_3 u_6 + P_6 A_6$	4.70	4.59	4.90	7.01	8.91	13.09	18.66
$\dot{m}_7 u_7 + P_7 A_7$	13.33	13.40	14.31	15.57	18.64	24.44	31.69
Input minus output, without separation	5.19	5.15	4.67	5.13	2.72	0.22	-1.01
x = fraction of A_5 carrying the flow	1	1	1	0.968	0.808	0.652	0.512
u_{5x}	-	-	-	4.53	4.26	3.87	3.29
$\dot{m}_1 u_{5x} + P_5 A_5$	-	-	-	13.96	14.15	14.56	15.76
Input minus output, with separation				5.40	4.42	3.21	2.73
P_{fr}	11.70	12.60	18.12	23.67	31.52	46.28	65.71
u_{fr}	3.27	3.06	2.20	1.70	1.29	0.88	0.62
$\Delta(\dot{m}_7 u_7 + P_7 A_7)_{fr}$	3.10	2.90	2.09	1.61	1.22	0.83	0.59
Input minus output, with separation and friction	2.09	2.25	2.58	3.79	3.20	2.38	2.14

d. Losses and gains of available energy in the driving fluid. Losses are negative, gains positive·

		45.1	45.5	45.9	45.13	45.17	45.21	45.25
Total change, Btu hr^{-1}		-32.22	-27.24	-24.63	-21.98	-18.66	-14.31	-10.40
Acceleration	%	-6.4	-5.0	-3.9	-6.1	-6.1	-5.9	-4.2
Mixing tube	%	-62.3	-75.5	-79.9	-86.1	-87.5	-88.5	-90.9
Mixing tube useful work	%	-2.3	-6.6	-8.6	-4.2	-4.9	-4.4	-3.5
Deceleration	%	-29.4	-11.8	-6.5	-2.1	-0.3	-0.5	-1.0
Deceleration useful work	%	+0.4	-1.1	-1.1	-1.5	-1.2	-0.7	-0.4
Total change	%	-100.0	-100.0	-100.0	-100.0	-100.0	-100.0	-100.0

e. Losses and gains of available energy in the driven fluid. Losses are negative, gains positive.

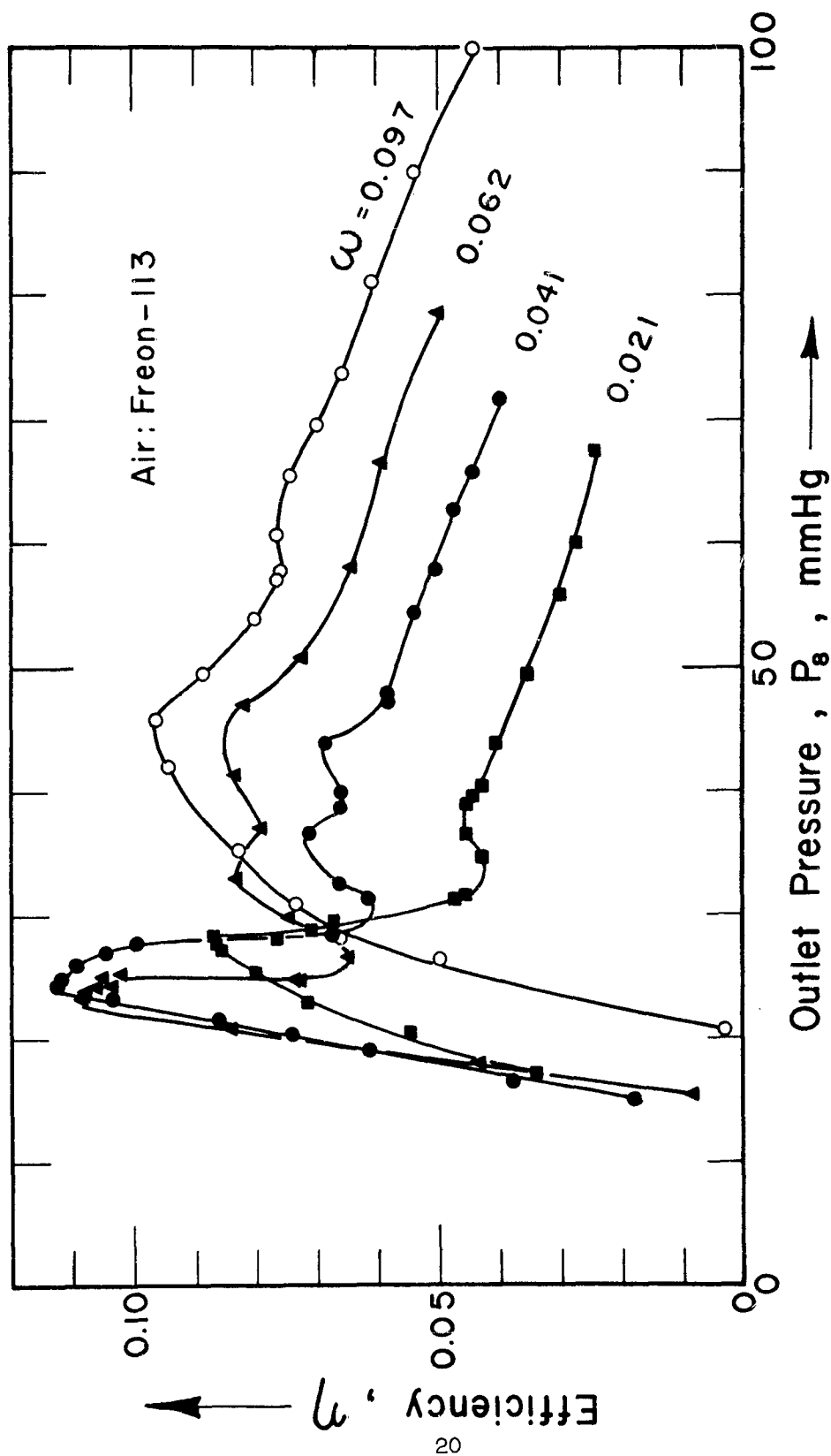|		45.1	45.5	45.9	45.13	45.17	45.21	45.25
Total change, Btu hr^{-1}		0.53	2.02	2.31	1.22	1.12	0.73	0.40
Acceleration	%	-16.8	-4.0	-2.9	-2.1	-1.4	-0.9	-0.5
Mixing tube	%	+139.8	+89.6	+91.1	+76.0	+81.5	+87.3	+90.4
Deceleration	%	-23.0	+14.4	+11.8	+26.1	+19.9	+13.6	+10.1
Total change	%	+100.0	+100.0	+100.0	+100.0	+100.0	+100.0	+100.0

Fig. 4. Efficiency η versus outlet pressure P_8, for half of the runs shown in Fig. 3.

show two peaks of maximum efficiency. The peak occurring at the lower value of P_8 is associated with the supersonic regime and the other is associated with the mixed regime. Evidence to confirm this statement is presented later.

Effect of Varying the Entrainment Ratio. After efficiency had been plotted against outlet pressure, the peak value or values of efficiency were read from each curve. The values thus obtained (designated η_{max}) are given in Table 2, along with the associated values of outlet pressure, entrainment ratio, and other relevant data. Table 2 contains all the runs made on each of the six systems studied. Note that every line of Table 2 represents an entire run. Since the specimen run 45 was only partially presented in Table 1, it is clear that a large body of experimental data is summarized in Table 2.

It is illuminating to plot from Table 2 a graph of maximum efficiency versus entrainment ratio. This has been done in Fig. 5. Each point in this figure represents the maximum (or one of the maxima) of a curve such as those in Fig. 4. Each curve is labeled to show the system of gases to which it refers. The graph has been drawn in two sections, so that the curves could be spread out and confusion avoided. Note that the two abscissa scales, which are logarithmic, have ranges that partially overlap.

Most of the curves have two branches. The branch identified by the letter S is associated with the supersonic regime of flow; the branch identified by the letter M is associated with the mixed regime. The curve for the system Freon-12:air has no supersonic branch. The system air:air has two supersonic branches, labeled S1 and S2 in Fig. 5. The S1 and S2 branches are discussed in Section 10.

Effect of Using Different Gases. In our previously-reported experiments we found that the efficiency attainable with a given system of gases was strongly influenced by their molecular-weight ratio. Low values of this ratio ($W_3/W_1 =$ driven/driving) were found to be associated with high efficiencies, and high values associated with low efficiencies. A similar dependence is shown by the data in Fig. 5.

Maximum values of efficiency were read from the curves of Fig. 5 and are given in Table 3, together with other data showing the conditions

TABLE 2. HIGHEST EFFICIENCIES ACHIEVED BY VARYING P_8 AT CONSTANT ω ($\eta = \eta_{max}$)

Run & Point	$\dot{m}$ lbm hr^{-1}	ω	η_{max}	P_1 mm Hg	P_3 mm Hg	P_8 mm Hg	P_8/P_1	P_8/P_3	P_8/P_5
a. He:Freon-113 (supersonic regime)									
61.6	2.474	0.0027	0.0843	152.0	11.5	27.91	0.1836	2.427	0.685
60.6	2.474	.0031	.1010	152.0	10.5	26.78	.1762	2.550	.611
58.6	2.474	.0043	.1243	152.0	10.5	25.11	.1652	2.391	.644
59.5	2.432	.0050	.1224	152.5	11.5	24.68	.1618	2.146	.610
62.5	2.482	.0073	.1228	152.5	14.0	24.32	.1595	1.737	.753
57.4	2.490	.0093	.1254	153.0	14.5	23.06	.1507	1.590	.845
63.3	2.482	.0124	.0854	152.5	16.5	21.32	.1398	1.292	.982
(mixed regime)									
61.16	2.474	0.0027	0.0448	152.0	26.0	39.51	0.2599	1.520	1.151
60.16	2.474	.0031	.0494	152.0	26.0	39.02	.2567	1.501	1.132
58.19	2.482	.0043	.0649	152.5	25.5	37.84	.2481	1.484	1.183
59.16	2.474	.0050	.0697	152.0	27.5	39.09	.2572	1.422	1.175
62.19	2.482	.0073	.0841	152.5	31.5	41.95	.2751	1.332	1.142
57.15	2.474	.0096	.0966	152.0	32.5	41.81	.2751	1.286	1.199
63.14	2.482	.0124	.1029	151.5	32.5	40.28	.2659	1.239	1.146
64.9	2.482	.0137	.1051	152.5	32.5	39.63	.2599	1.219	1.184
65.10	2.482	.0168	.0996	152.5	39.5	45.55	.2987	1.153	1.140
56.5	2.482	.0214	.0892	152.5	39.5	43.83	.2874	1.110	1.220
b. He:air (supersonic regime)									
35.4	2.501	0.0167	0.0684	367.0	25.5	52.87	0.1441	2.073	0.683
34.11	2.501	.0246	.0736	370.5	29.0	50.74	.1370	1.750	.729
30.3	2.501	.0362	.0782	369.0	37.5	55.99	.1517	1.493	.869
(mixed regime)									
34.18	2.497	0.0245	0.0508	368.5	50.0	74.12	0.2011	1.482	1.073
71.10	2.488	.0517	.0713	368.5	46.5	68.31	.1854	1.469	1.072
30.19	2.510	.0565	.0757	365.0	63.0	86.50	.2370	1.373	1.088
31.11	2.510	.0434	.0827	369.0	65.0	84.84	.2299	1.347	1.089
69.11	2.497	.0640	.0928	372.0	63.5	80.46	.2163	1.267	1.107
32.11	2.510	.0749	.0965	371.0	82.5	99.56	.2684	1.207	1.092
70.14	2.501	.0900	.0976	373.0	105.0	120.82	.3239	1.151	1.130
33.11	2.499	.1315	.0760	371.5	112.0	120.79	.3251	1.078	1.166

Run & Point	$\dot{m}$ lbm hr^{-1}	ω	η_{max}	P_1 mm Hg	P_3 mm Hg	P_8 mm Hg	P_8/P_1	P_8/P_3	P_8/P_5
				c. air:Freon-113 (supersonic regime)					
42.7	2.474	0.0210	0.0872	152.0	11.5	28.13	0.1851	2.446	0.670
54.5	2.482	.0254	.0978	152.5	11.0	26.20	.1718	2.382	.578
39.5	2.482	.0304	.1136	152.5	11.5	26.60	.1744	2.313	.677
73.5	2.475	.0323	.1047	152.0	11.5	24.68	.1624	2.146	.607
53.5	2.474	.0360	.1084	152.0	12.0	24.56	.1616	2.047	.625
45.7	2.490	.0413	.1127	153.0	12.5	24.22	.1583	1.938	.666
38.2	2.499	.0489	.1148	153.5	14.5	25.47	.1659	1.757	.738
55.5	2.482	.0544	.1177	152.5	14.5	24.62	.1614	1.698	.785
51.4	2.474	.0622	.1090	152.0	15.0	23.40	.1540	1.560	.774
37.16	2.475	.0640	.1110	152.0	15.5	23.96	.1576	1.546	.785
43.4	2.509	.0657	.1074	154.0	15.5	23.54	.1529	1.519	.790
				(mixed regime)					
42.13	2.501	0.0207	0.0456	153.5	25.5	38.81	0.2528	1.522	1.109
54.10	2.474	.0253	.0539	152.0	24.0	36.53	.2403	1.522	1.144
39.10	2.482	.0299	.0571	152.5	23.5	34.76	.2279	1.479	1.113
73.12	2.475	.0310	.0609	152.0	24.5	36.22	.2383	1.478	1.110
53.14	2.474	.0359	.0674	152.0	25.0	36.33	.2390	1.453	1.137
45.15	2.474	.0411	.0714	152.0	26.0	36.71	.2415	1.412	1.149
38.3	2.475	.0492	.0782	152.0	26.0	35.86	.2359	1.379	1.119
55.9	2.482	.0543	.0820	152.5	25.0	34.28	.2248	1.371	1.113
51.16	2.482	.0611	.0837	152.5	32.0	41.28	.2707	1.290	1.213
37.5	2.475	.0644	.0886	152.0	32.5	41.84	.2753	1.287	1.189
43.15	2.482	.0656	.0888	152.5	32.0	41.18	.2700	1.287	1.228
40.6	2.490	.0739	.0932	153.0	32.5	41.16	.2690	1.266	1.222
36.14	2.467	.0970	.0964	151.5	38.5	45.73	.3018	1.188	1.232
41.5	2.467	.1119	.1002	151.5	34.5	40.85	.2696	1.184	1.267
50.3	2.460	.1186	.0970	151.0	36.0	41.89	.2774	1.164	1.242
52.7	2.501	.1226	.0922	153.5	36.0	41.50	.2704	1.153	1.251
44.6	2.467	.1305	.0895	151.5	37.5	42.55	.2809	1.135	1.254

TABLE 2. (Continued)

Run & Point	ṁ lbm hr⁻¹	ω	η_{max}	P_1 mm Hg	P_3 mm Hg	P_8 mm Hg	P_8/P_1	P_8/P_3	P_d/P_5
				d. air:Freon-12 (supersonic regime)					
67.6	2.514	0.0247	0.0708	193.0	13.0	33.51	0.1736	2.578	0.567
17.8	2.598	.0279	.0785	195.5	13.0	33.21	.1699	2.555	.574
47.7	2.483	.0401	.0911	190.5	13.5	30.13	.1582	2.232	.608
46.6	2.483	.0507	.0982	192.0	15.0	30.14	.1570	2.009	.643
49.5	2.489	.0589	.1055	190.0	15.5	29.72	.1564	1.917	.713
9.8	2.514	.0605	.1036	190.5	16.5	30.63	.1608	1.856	.721
66.5	2.523	.0609	.1035	194.5	16.5	30.63	.1575	1.856	.714
12.3	2.514	.0702	.1004	189.5	17.5	29.67	.1566	1.695	.743
11.4	2.514	.0834	.0914	190.5	19.0	28.86	.1515	1.519	.790
48.5	2.495	.0890	.0885	190.5	18.5	27.35	.1436	1.478	.776
				(mixed regime)					
67.13	2.514	0.0246	0.0373	194.0	29.0	45.63	0.2352	1.573	1.095
47.13	2.489	.0399	.0543	190.5	29.0	43.88	.2303	1.513	1.095
46.13	2.483	.0505	.0645	192.5	28.0	41.90	.2177	1.496	1.102
49.16	2.495	.0585	.0676	199.0	29.5	42.36	.2230	1.436	1.134
66.12	2.523	.0606	.0698	194.5	32.0	45.44	.2336	1.420	1.148
12.6	2.526	.0695	.0745	189.0	36.5	49.49	.2618	1.356	1.156
11.9	2.514	.0825	.0808	189.0	36.5	48.45	.2564	1.327	1.152
48.18	2.495	.0883	.0848	190.0	40.0	52.17	.2746	1.304	1.188
13.7	2.552	.1059	.0889	193.5	37.5	48.08	.2485	1.282	1.164
10.5	2.511	.1256	.0936	191.0	44.0	53.93	.2824	1.226	1.192
16.4	2.565	.1463	.0981	195.5	42.0	50.98	.2608	1.214	1.193
14.5	2.539	.1659	.0933	192.5	44.0	51.58	.2680	1.172	1.202
15.5	2.549	.2278	.0757	192.0	56.5	61.45	.3200	1.088	1.237

24

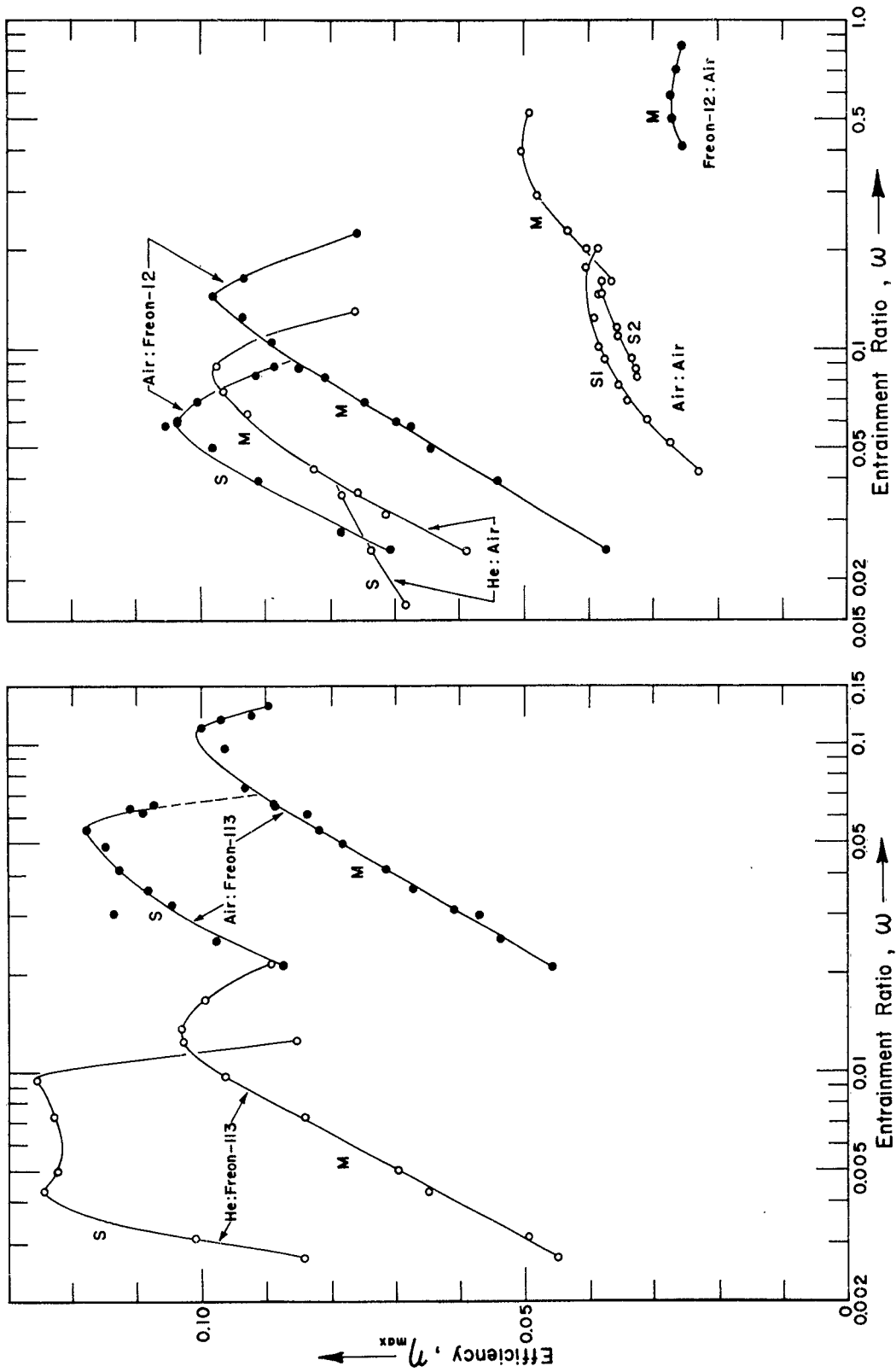| Run & Point	$\dot{m}$ lbm hr^{-1}	ω	η_{max}	P_1 mm Hg	P_3 mm Hg	P_8 mm Hg	P_8/P_1	P_8/P_3	P_8/P_5
					e. air:air (supersonic regime)				
81.8	1.270	0.0423	0.0230	191.5	15.5	31.03	0.1620	2.002	0.702
76.8	1.280	.0520	.0273	194.0	16.0	31.46	.1622	1.966	.727
79.6	1.266	.0609	.0307	190.5	16.0	30.71	.1612	1.920	.649
77.6	1.270	.0697	.0339	195.5	16.5	31.11	.1591	1.886	.702
78.4	1.273	.0780	.0353	192.0	16.5	30.01	.1563	1.819	.716
80.5	1.263	.0824	.0323	193.0	17.5	29.61	.1534	1.692	.804
72.4	1.276	.0877	.0326	191.5	17.0	28.26	.1476	1.662	.794
74.5	1.256	.0929	.0376	188.0	16.5	28.45	.1513	1.724	.706
75.9	1.285	.0938	.0333	193.0	18.0	29.16	.1511	1.620	.831
84.4	1.263	.1016	.0385	190.0	17.5	29.15	.1534	1.666	.721
82.4	1.271	.1096	.0555	191.0	18.5	28.82	.1509	1.558	.833
85.7	1.270	.1165	.0356	193.0	20.0	30.25	.1567	1.513	.911
19.6	1.266	.1254	.0392	193.0	20.5	31.14	.1614	1.519	.758
88.4	1.273	.1308	.0385	192.0	20.0	29.86	.1555	1.493	.771
86.8	1.273	.1478	.0779	192.5	23.0	32.34	.1680	1.406	.958
87.10	1.270	.1615	.0779	193.0	26.5	35.78	.1854	1.350	1.044
20.7	1.273	.1784	.0404	194.0	26.5	35.48	.1829	1.339	1.005
83.9	1.263	.2036	.0386	191.0	26.0	33.42	.1750	1.285	1.023
					(mixed regime)				
87.13	1.270	0.1614	0.0365	193.0	34.5	44.75	0.2319	1.297	1.053
83.15	1.261	.2044	.0403	190.0	35.5	42.29	.2226	1.262	1.054
21.10	1.270	.2297	.0431	193.5	49.5	59.43	.3071	1.201	1.053
22.12	1.280	.2953	.0478	192.0	49.5	58.09	.3026	1.174	1.054
23.9	1.253	.4034	.0503	191.0	59.0	65.97	.3454	1.118	1.050
24.4	1.250	.5319	.0492	194.0	59.5	64.83	.3342	1.090	1.050
					f. Freon-12:air (mixed regime)				
25.10	2.480	0.4161	0.0256	365.5	50.0	69.69	0.1907	1.394	1.079
26.8	2.488	.5084	.0271	362.5	71.0	90.37	.2493	1.273	1.112
27.8	2.497	.5926	.0274	361.0	68.0	84.63	.2344	1.245	1.108
28.6	2.463	.7075	.0266	367.5	72.0	86.39	.2351	1.200	1.134
29.5	2.471	.8363	.0258	365.5	78.0	90.17	.2467	1.156	1.134

Fig. 5. Maximum efficiency (η_{max}) versus entrainment ratio ω. Each plotted point is the maximum value from a curve such as those in Fig. 4.

TABLE 3. HIGHEST EFFICIENCIES ACHIEVED BY VARYING BOTH P_8 AND ω ($\eta = \eta_2$).

| System | | Supersonic Regime | | | | Mixed Regime | | | |
(Driven:Driving)	W_3/W_1	Run & Point	ω	P_8/P_3	η_2	Run & Point	ω	P_8/P_3	η_2
He:Freon-113	0.02137	57.4	0.0093	1.590	0.1254	64.9	0.0137	1.219	0.1031
He:air	.1382	----	------	-----	------	70.14	.0900	1.151	.0976
Air:Freon-113	.1546	55.5	.0544	1.698	.1177	41.5	.1119	1.184	.1002
Air:Freon-12	.2396	49.5	.0589	1.917	.1055	16.4	.1463	1.214	.0981
Air:air	1	----	------	-----	------	23.9	.4034	1.118	.0503
Freon-12:air	4.174	----	------	-----	------	27.8	.5926	1.245	.0274

under which the maxima were achieved. The procedure followed was similar to that applied to the curves of the type of Fig. 4, which yielded the values of η_{max} plotted in Fig. 5. The maximum values found from Fig. 5 are designated η_2 to indicate that they result from maximizing the efficiency with respect to two variables: P_8 and ω.

The value of η_2 for each system of gases is plotted in Fig. 6 against the molecular-weight ratio of the gases. For the present apparatus there are two curves, designated S and M respectively; the S indicates results obtained in the supersonic regime and the M indicates results obtained in the mixed regime. For comparison, the results obtained with our previous apparatus are included. The curve representing these results is designated M because it corresponds to the mixed regime. The supersonic regime was not observed in the earlier work; hence the figure contains no S-curve for the earlier apparatus.

5. Comparison of Present and Previous Results

In our earlier experiments, the supersonic regime of flow was never attained. After this regime had been observed and studied in the present apparatus, attempts were made to establish it in the first apparatus, but without success. The supersonic regime is most readily established at low entrainment ratios (or at zero entrainment). In this condition the driving fluid continues to expand outside its nozzle.

The amount of expansion required to fill the mixing tube with supersonic flow depends on the area ratio A_7/A^*, in which A_7 is the mixing-tube cross section, and A^* is the cross section of the throat of the driving-fluid nozzle. The second apparatus, which was used in the present measurements, had $A_7/A^* = 7.00$. The first apparatus had $A_7/A^* = 9.93$. Apparently this difference was great enough so that the supersonic regime could be established easily in the second apparatus and not at all in the first. The outlet pressure P_8 is also a limiting factor, but it was produced by the same vacuum pump in both cases. Presumably if a pump of higher capacity had been available, so that lower values of P_8/P_1 could have been reached, it would have been possible to establish the supersonic regime in both apparatuses.

Another factor that may have contributed to the difficulty of establishing supersonic flow in the first apparatus was the fact that most of
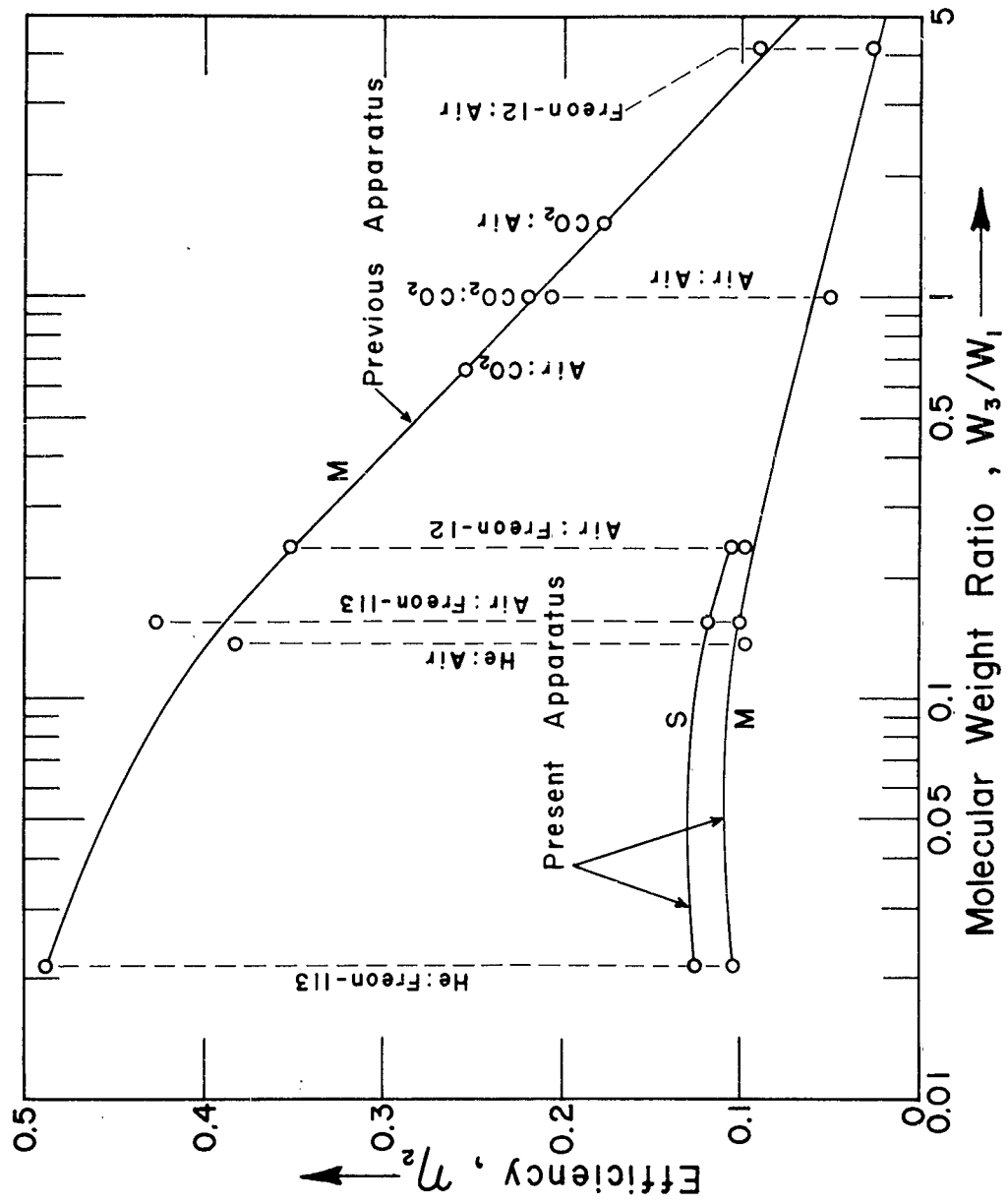
Fig. 6. Maximum efficiency (η_2) versus molecular-weight ratio (driven/driving) of the gases employed. Each plotted point represents the maximum efficiency found by varying both P_8 and ω.

the necessary expansion to fill the mixing tube would have had to take place outside the driving-fluid nozzle. For the first apparatus A_5/A^* was 1.42, in comparison to 2.30 for the second apparatus. Expansion inside a nozzle that guides the flow may involve less loss than expansion where the stream is surrounded by stagnant or slow-moving gas.

As may be seen in Fig. 6, the highest efficiency achieved with the present apparatus was 0.125; this is only one fourth the high of 0.489 achieved with the previous apparatus. However, the previous high was attained at a compression ratio of only 1.065, while the present high was attained at a compression ratio of 1.590. A ratio of 1.065 would be useful only in ventilation or other gas-moving applications. A ratio of 1.590, while still low, is much nearer to the requirements of most jet-compressor applications.

The high efficiencies and low compression ratios obtained with the first apparatus appear to be associated with a relatively small mismatch in the velocities of the driving and driven streams. The greater mismatch in velocity found in the present apparatus is associated with a larger value of the area ratio A_5/A^* and a smaller value of the area ratio A_6/A_5, than that of the first apparatus. Also, in the present apparatus the maximum efficiencies occurred at lower entrainment ratios than in the first apparatus.

In the first apparatus A_6/A_5 was 5.97; in the present apparatus it was 2.04. Presumably if this ratio were reduced still further the trend toward greater velocity mismatch, higher compression ratio, lower efficiency, and lower entrainment ratio at maximum efficiency would continue.

6. Identification of the Various Regimes of Flow

The experimental results presented thus far are mainly compression ratios and efficiencies. These quantities are based on measurements made outside the jet compressor. We have referred to various regimes of flow in the course of the presentation, but the compression ratios, expansion ratios, and efficiencies are independent of any assumptions regarding what happens inside the jet compressor.

We will now examine the pressure-patterns that exist inside the ejector and show how they permit the various regimes of flow to be identified.

Figure 7 shows pressures measured within the apparatus during the specimen run 45. These pressures have been normalized by dividing by the driving-fluid initial stagnation pressure P_1, and P/P_1 has been plotted as a function of position within the apparatus. A drawing at the top of the figure shows the locations of the various pressure taps. Both views are drawn to the scale of the graph below, except that in the lower view, where the depths of the flow channels are shown, the vertical scale has been doubled to improve clarity.

The supersonic regime, which we characterized as one in which changes in downstream conditions have no appreciable influence on upstream conditions, is represented in Fig. 7 by points 45.1 and 45.5. Note that between these two points the outlet pressure P_8 has been raised substantially, but there has been no change in the upstream pressure distribution. (The small constant displacement of curve 45.5 from 45.1 from tap b to tap h is not significant. It results from the nature of the manometric system. Pressure P_3 was read on a mercury manometer. All other pressures except P_1 and P^* were read on an oil manometer which gave $P - P_3$. Hence a change or an error in P_3 could shift an entire curve upward or downward.) When upstream pressures are independent of downstream pressures, we know that the supersonic (or possibly the saturated supersonic) regime exists.

Curve 45.9, which lies next above the two curves just discussed, is near the limit of the supersonic regime. The isolation of the upstream portion of the driven stream from downstream influence is beginning to break down. The rise in P_8 has definitely affected the pressure at tap h, and the curve extending back to tap b (where P_3 is measured) has been raised by an amount somewhat greater than the uncertainty of measurement (0.5 mm Hg change in the reference pressure can be detected). It will be recalled that both the mixed regime and the mixed regime with separation are characterized by a coupling between P_8 and P_3, so that the two pressures rise and fall together.

Curve 45.13 is far within the mixed regime. In fact, as will be shown later, separation is incipient at this point. In the present experiments, separation has been deduced from calculations of momentum-flux balance, and separation has been assumed where the balance conditions could not be satisfied without some such assumption. Observed values of the pressure P_5 at the driving-nozzle exit confirm the assumed separation. Separation within the driving-fluid nozzle definitely occurs
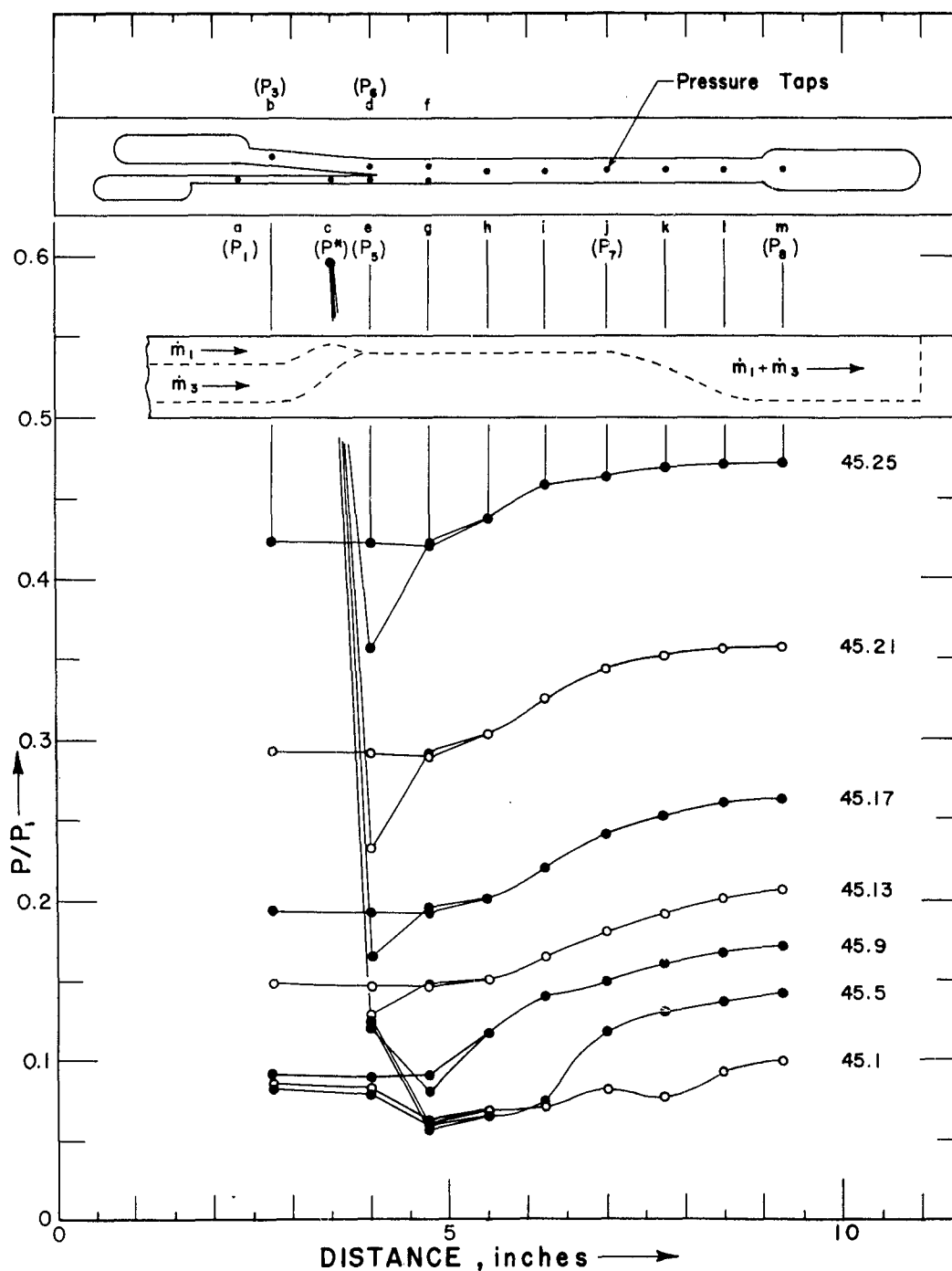
31

Fig. 7. Pressure variation along the flow channels in run 45. The abscissa is distance measured from the inlet end of the flat bar. The ordinate is pressure divided by the corresponding inlet pressure. A drawing of the flat bar and the flow channels cut in it is given at the top.

for curve 45.17 and for the two curves lying above it. In the mixed regime, and the mixed regime with separation, the pressure difference $P_8 - P_3$ remains roughly constant as the two pressures increase.

The saturated supersonic regime does not appear in Fig. 7. Our evidence for this fact is obtained by calculating u_6, the velocity of the driven stream at the beginning of mixing. This velocity, calculated from the observed pressure P_6, is given in Table 1, part c. The sonic velocity c^* that the stream would reach in choked flow is 6.51 $Btu^{\frac{1}{2}}$ $lbm^{-\frac{1}{2}}$. This value was calculated on the assumption that the stagnation temperature (room-temperature) of the air was $530°R$. The calculated values of u_6 in Table 1 are all well below c^*.

Unless the downstream pressure is very low - lower than it would ever be in an ejector operating at good efficiency - there is always more or less subsonic flow in the downstream portion of the mixing tube. When the supersonic regime exists, the conversion to subsonic flow within the mixing tube takes place in an extended shock. In point 45.1, Fig. 7, there is a slight rise in pressure between taps i and j, which may be the result of friction, or possibly the beginning of an extended shock. In point 45.5 the rise is much more noticeable, and is clearly the beginning of an extended shock. In point 45.9 the extended shock has been pushed farther upstream by the higher value of P_8. The rise in pressure has penetrated upstream to taps f and g, and the attached supersonic flow is about to be "pried loose" from the mixing-tube walls by the subsonic flow and boundary layer associated with the extended shock.

It is instructive to look at Fig. 3 and note the relationship between the shape of the compression-ratio curve and the change from one flow regime to another. According to Fig. 7, point 45.9 shows the beginning of breakdown of the supersonic regime into the mixed regime. In Fig. 3, the specimen run 45 may be identified by its entrainment ratio (0.041). Point 45.9 is the ninth point of this run, in order of increasing P_8, and lies slightly beyond the supersonic maximum. Point 45.13, which is near the dividing line between the mixed regime and the mixed regime with separation, lies at the bottom of a small minimum in the compression-ratio curve.

The transition from the supersonic to the mixed regime is sometimes continuous, as it was in the specimen run 45. In such a case it is

possible with care to obtain measurements at any point on the compression-ratio curve (Fig. 3). In other cases the transition is discontinuous and a portion of the right-hand side of the supersonic peak is unrealizable. Sometimes hysteresis is observed and the curve has two branches that overlap for a small range of P_8. When this range is approached by increasing P_8 the supersonic range persists, and when it is approached by decreasing P_8 the mixed regime persists.

The division between the supersonic and mixed regimes is at the discontinuity if one exists. Where no discontinuity exists, we have somewhat arbitrarily placed the division at the value of P_8 at which the curve of P_8/P_3 has fallen halfway from its supersonic maximum to the following minimum.

In Fig. 3, the three curves of highest entrainment ratio show no supersonic maxima. This is not unexpected. The driven fluid enters the mixing tube relatively slowly, usually at a velocity less than 1/4 of c^*, its sonic velocity in choked flow. At high entrainment ratios the driving stream is not able to raise the mixture to supersonic velocity (or to produce the conditions where the generalized choking noted by Pearson, Holliday, and Smith (6) occurs).

. The rise in pressure between taps g and j, shown by most of the curves in Fig. 7, has been explained for curves 45.1, 45.5, and 45.9 as due to an extended shock in the downstream portion of the mixing tube. The four remaining curves lie in the mixed regime and the mixed regime with separation, yet they also show the rise in pressure. The pressure rise in these curves is due to the conversion of the supersonic core of flow to the subsonic state, by a mechanism somewhat similar to an extended shock.

It is possible for a pressure rise to continue in the mixing tube after all of the flow is subsonic. Such a pressure rise can occur as a result of equalization of velocity, as a higher-speed core shares its momentum with lower-speed flow near the mixing-tube walls. The effect must of course be large enough to overcome the natural pressure drop in subsonic flow due to friction.

7. Momentum-Flux Balance

As a test of the picture of jet-compressor operation presented above, calculations were made to see if the momentum equation was

satisfied. We define equivalent momentum-flux as the sum of the true momentum flux $\dot{m}u$ and the pressure force PA. Then, in a constant-area control volume such as those illustrated in Fig. 1, input must equal output plus friction loss. Any unbalance not attributable to friction must be attributed to an incorrect picture of the process and resulting incorrect calculated values. The equations of energy and continuity must also be satisfied, but they offer few problems. The gases may suffer a slight gain or loss of heat as they pass through the ejector, but in a previously-reported investigation (1) this was found to be negligible and heat transfer is believed to be unimportant in the present work.

Input and output equivalent momentum-flux have been computed for certain selected runs. A simple calculation based on one-dimensional flow of all streams gives a fairly good balance between input and output in some regions of operation, when friction is taken into account. In other regions of operation it is necessary to assume some mechanism such as separation in order to calculate a reasonable equivalent momentum-flux balance.

One-Dimensional Calculation Without Separation. Consider a control volume bounded by the walls of the mixing tube (Fig. 1), the entrance plane 5,6 and the exit plane 7. Ignoring friction, the momentum-flux equation for this volume is

$$\dot{m}_7 u_7 + P_7 A_7 = \dot{m}_1 u_5 + P_5 A_5 + \dot{m}_3 u_6 + P_6 A_6. \qquad (3)$$

The pressures P_5, P_6, and P_7 are all known from measurement. Applying the equations of continuity and energy and the ideal gas law, the velocities u_5, u_6, and u_7 can be calculated from the corresponding pressures. For one-dimensional flow

$$u = -y + \left(y^2 + 2\, c_p\, T_0\right)^{\frac{1}{2}} \qquad (4)$$

where $y = PAc_p/\dot{m}R$, T_0 is the stagnation temperature of the stream, and R is its gas constant.

Calculations based on Eq. (3) and (4) have been made for runs 16, 19, 23, 45, and 49. Results for the specimen run 45 are given in Table 1, part c. Units of the various quantities are given in the table, and the conversion factor $14.155 \text{ in}^{-2} (\text{mm Hg})^{-1} \text{Btu}^{\frac{1}{2}} \text{lbm}^{\frac{1}{2}} \text{hr}^{-1}$

has been used where necessary. The input and output are plotted as solid lines in Fig. 8a. Part b of the figure shows similar calculations made for run 19. For both runs the solid curves cross, showing that, on a one-dimensional basis, the calculated output becomes greater than the calculated input.

When input exceeds output, the difference can be attributed at least in part to friction, but when output exceeds input we know that the calculated results are in error. Runs 16, 23, and 49 also showed an excess of momentum-flux output over input for part or all of the range of P_8. Hence it was necessary to look for a flow pattern that would give either a lower output or a higher input than simple one-dimensional flow without separation.

Calculation with Separation Assumed. The most plausible way to remove the paradox of calculated output exceeding calculated input is to assume separation in the driving-fluid nozzle. When separation occurs, the supersonic stream separates from the walls of the nozzle at some plane lying between the throat and the exit plane of the nozzle, as shown in the third diagram of Fig. 1. Equation (3) which assumes one-dimensional flow in A_5, A_6, and A_7, may be applied in the supersonic and mixed regimes, but not if separation occurs.

The assumption that separation exists must be made quantitative in some way. That is, we must make a model of the separated flow from which numerical computations of input momentum-flux can be made. First we will imagine a cone lying within the diverging part of the driving fluid nozzle. This cone joins the nozzle walls at the plane of separation and extends to the nozzle exit plane A_5. This imaginary cone carries all of the net flow after separation. Its exit area is xA_5 where x is a fraction that can never exceed 1.

Next we will assume that the flow in the imaginary cone, after separation exists, bears the same relation to isentropic flow as exists in the nozzle when separation does not occur. This assumption will permit us to calculate x from the observed pressure P_5. Furthermore, it will permit separated flows and unseparated flows to be calculated in such a way that there is no discontinuity, but a smooth transition from unseparated to separated flow.

In the one-dimensional calculations of state 5 just completed, isentropic flow was not assumed. State 5 was calculated from Eq. (3)
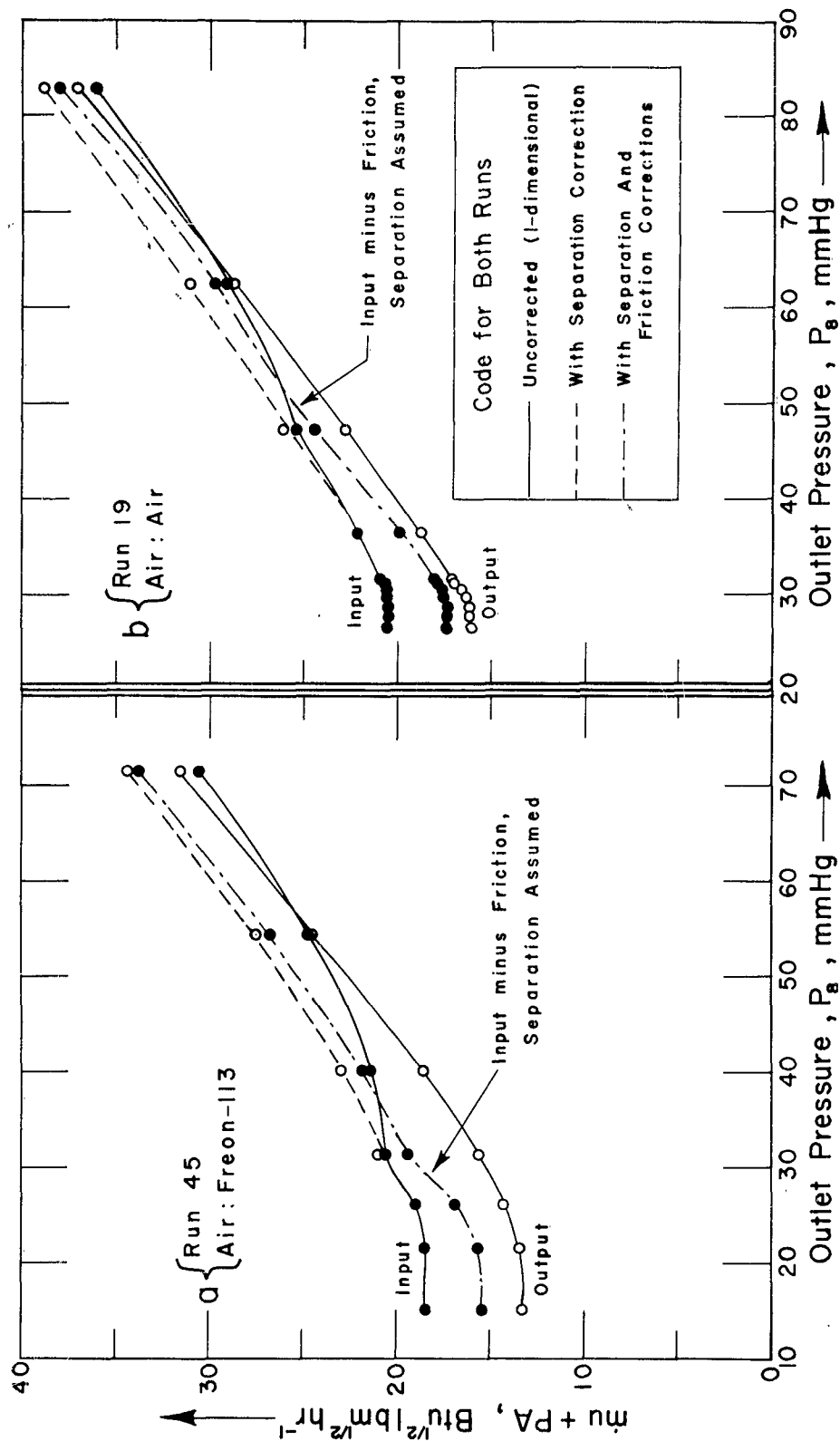
36

Fig. 8. Equivalent momentum-flux for runs 45 and 19, shown as a function of outlet pressure, and according to various modes of calculation.

and (4), which involve the equations of energy and continuity, and the observed pressure. An isentropic calculation of state 5 can be made from the nozzle area-ratio A_5/A^*, that yields the isentropic expansion ratio P_{5s}/P_1. From this and the actual expansion ratio P_5/P_1, the ratio P_{5s}/P_5 can be calculated. This ratio remains fairly constant as long as separation does not occur. In run 45 (Table 1), $P_6/P_5 < 1$ for the first three points, and for these, separation should certainly not occur. Their average value of P_5/P_1 is 0.1227. The isentropic value P_{5s}/P_1 (at $A_5/A^* = 2.30$) is 0.1160, whence $P_{5s}/P_5 = 0.95$.

All points for which $P_6/P_5 > 1$ were considered subject to possible separation, and for them, using the observed value of P_5 and the accepted value of P_{5s}/P_5, values of P_{5s} and P_{5s}/P_1 were calculated. Then an area xA_5 was calculated, such that it would carry the isentropic "reference flow" at the calculated value of P_{5s}/P_1. The area xA_5 was taken as the exit area of the imaginary cone to which the separated flow was confined. Once a value of x had been found, the isentropic reference flow had served its purpose and no further use was made of it.

Values of x, the fraction of A_5 occupied by the separated flow, calculated for run 45 as described above, are given in Table 1, part c. The input velocity u_{5x} was calculated from them, using Eq. (4) just as in the earlier one-dimensional calculation, except that the area used was not A_5 but xA_5. The velocity u_{5x} is higher than the one-dimensional velocity u_5 because of the smaller area carrying the flow. It is this increase which, as will be seen, avoids the earlier impossible situation wherein calculated output was greater than calculated input. The pressure term P_5A_5 has been assumed unchanged by the separation. It is likely that the annular space around the core, with area $(1-x)A_5$, has a pressure somewhat higher than P_5, perhaps approaching P_6, but this has not been taken into account.

The results of modifying the momentum-flux calculations for run 45, by assuming separation as outlined above, are given in Table 1, part c, and are plotted in Fig. 8a, where they are represented by a dashed line. The assumption of separation has had the desired effect of raising the calculated input in the region of high P_8-values. The input and output curves are made more nearly parallel, and input is now always greater than output. The remaining discrepancy is of the

proper sign to be explained by friction. An estimate of the loss of momentum flux to be expected from friction is given below.

Calculations based on separated flow were also made for run 19, and are shown in Fig. 8b. Here also the assumption of separation brought input momentum flux above output throughout the run. For run 19 (air:air), P_{5s}/P_5 was only 0.53, as compared with 0.95 for run 45 (air:Freon-113), indicating much greater losses in air than in Freon-113 within the driving-fluid nozzle. The slower-moving Freon should be more nearly isentropic than air, but the difference between the two gases seems rather large.

The three other runs (16, 23, 49) that showed outputs exceeding inputs on the one-dimensional basis were recalculated with separation assumed, and the discrepancies were satisfactorily removed. For runs 16 and 23, separation was present throughout the run, so for them the factor P_{5s}/P_5 had to be taken from another run on the same system.

Pressure Ratio Required to Cause Separation. It is of interest to find the value of the pressure ratio P_6/P_5 when separation begins to occur. Our criterion is the value of x; when x is near 1 there is no separation, but when x is significantly less than 1, separation is present. The values of x given in Table 1 show that, in run 45, separation was beginning to appear at point 45.13, for which $P_6/P_5 =$ 1.144. In run 19, separation had begun at $P_6/P_5 = 1.114$; in run 49, at 1.118. Runs 16 and 25 give no corresponding information, because separation was present throughout each run.

The criterion for separation is an indirect one, which we have justified by showing that it permits the equivalent momentum-flux equation to be satisfied. According to it, separation within the driving-fluid nozzle is already evident at $P_6/P_5 = 1.125$ and may begin as early as $P_6/P_5 = 1.1$. This value seems low. Summerfield, Foster, and Swan (8), for example, report for a rectangular channel that the pressure before separation was 0.38 to 0.41 of the downstream pressure, whence separation should occur at $P_6/P_5 =$ about 2.5. The small size of our apparatus increases the importance of boundary-layer effects; this may be the explanation of the low value of P_6/P_5 we observe at the onset of separation.

Friction in the Mixing Tube. Frictional losses originate at the mixing-tube walls and depend on the nature of the flow in the

immediate neighborhood of the walls. It is impossible to make an accurate calculation of friction for the conditions that exist within a mixing tube, because we do not know the precise velocity of flow near the wall. However, a rough calculation that gives little more than the order of magnitude of frictional losses is still of interest. We have seen that the momentum-flux calculation in which separation is assumed places the output well below the input over the entire range of outlet pressures, and we wish to know if friction could reasonably account for the difference.

The usual treatment of friction is based on the dimensionless friction factor defined as

$$f \equiv \frac{\sigma}{\frac{1}{2} \rho u^2} \tag{5}$$

in which σ is the shearing wall-force per unit area and ρ is fluid density. Values of f may be obtained from published graphs which give it as a function of Reynolds number.

Published friction factors refer to developed flows, in which the conditions at the walls are determined by the conditions throughout the entire stream. The flow in the mixing tube is far from being a developed flow; nevertheless we will make friction calculations in the conventional way.

The loss of equivalent momentum flux due to friction, in a length dl of channel having a perimeter B is

$$d \left(\dot{m} u + PA \right) = \sigma B \, dl.$$

Applying this to the mixing tube of finite length Δl, using Eq. (5) and the equation of continuity, the friction loss between plane 5,6 and plane 7 is

$$\Delta \left(\dot{m}_7 u + PA_7 \right) = \frac{1}{2} \frac{B_7}{A_7} \, f \, \dot{m}_7 \, u_{fr} \Delta l. \tag{6}$$

An average pressure P_{fr} along the length of the mixing tube was used in Eq. (4) to compute u_{fr}, the stream velocity to be used in the calculation of friction loss.

The viscosity of Freon-113 within the mixing tube was taken to be 0.0101 centipoise at the temperature of run 45, deduced from a value given by a manufacturer (9). This and the known viscosity of air permitted the Reynolds number to be calculated for run 45. The value found was 5200. Consulting the graph given by McAdams (10), the friction coefficient at this Reynolds number is 0.0092. Substituting this and other known values in Eq. (6) gives for the friction loss in run 45

$$\Delta \, (\dot{m}_7 \, u + PA_7) = 0.368 \, \dot{m}_7 \, u_{fr}. \tag{7}$$

Calculations of friction for run 45 are given in Table 1, part c. The input equivalent momentum-flux corrected for separation (dashed line in Fig. 8a) has been further corrected by subtracting the friction loss, and is plotted as a dot-dash curve in Fig. 8a. Figure 8b shows similar calculations made for run 19.

Friction calculations similar to those made for runs 45 and 19 were also made for runs 16, 23, and 49. The results in all cases were similar: the correction for friction reduced the discrepancy between calculated input and output equivalent momentum-flux, but was not large enough to produce good agreement.

Discussion of Equivalent Momentum-Flux Balance. When friction and separation are allowed for, the output is, in all cases for which calculations were made, substantially below input. An increase in the allowance for friction would improve the agreement between input and output. There is no obvious reason for increasing the allowance for friction loss, however, because in calculating the correction the actual flow was treated as if it were a developed flow. The losses in a developed flow may be expected to be greater than those in the actual flow.

The agreement between input and output equivalent momentum-flux shown in Fig. 8 may be as good as we should expect. The remaining discrepancy may be due to the assumption of one-dimensional flow in state 7. If the velocity of flow is assumed to be nonuniform, with the core moving faster than the gas near the walls, the computed equivalent momentum-flux is increased. By assuming the appropriate degree of nonuniformity, the agreement between input and output equivalent momentum-flux could be made very good.

It is doubtful, however, if any further refinements in momentum-flux calculations are justified. There is strong evidence that separation exists and that a separation correction should be made, but the way in which this correction has been made is somewhat arbitrary. Other workers might with equal justification make a correction in a somewhat different way, and might obtain either a larger or a smaller correction than the one we have calculated.

Since separation or nonuniform flow has been considered for states 5 and 7, it may be asked if the one-dimensional assumption is adequate for state 6, which refers to the driven fluid as it enters the mixing tube. Examination of the computed values of $\dot{m}_3 u_6$ and $P_6 A_6$ shows that the velocity term is very small compared to the pressure term, so that a change in assumed velocity distribution would have very little effect on the sum of the two terms.

Figure 8 shows that the agreement between calculated input and output is somewhat better for run 19 (air:air) than for run 45 (air:Freon-113). Run 23 (air:air) showed good agreement. Runs 16 and 49 (air: Freon-12) showed somewhat poorer agreement than run 45.

8. Allocation of Losses

If the losses within a jet compressor are to be reduced, it is important to know precisely where within the jet compressor the losses occur. The functioning of a jet compressor may be broken down into four processes as follows:

1. Acceleration of the driving stream.
2. Acceleration of the driven stream.
3. Mixing of the two streams.
4. Deceleration of the mixed stream.

In the preceding sections of this paper a way was found to calculate the fluid states immediately prior to mixing (states 5 and 6) and the state immediately after mixing (state 7) so as to satisfy the momentum-flux equation with fairly good accuracy. The calculated states 5, 6, and 7 can therefore be accepted with some confidence as fairly good approximations to the true states of the fluids. The initial states (1 and 3) and the final state (8) are stagnation states and are well known.

42

The loss or change in each of the four processes listed above has been calculated for the specimen run 45 and for the air:air run 19. The analysis has been made by computing the changes in available energy that occur during the various processes taking place in the jet compressor. The available energy a of unit mass of fluid in steady flow, relative to a dead state characterized by the subscript d, is (reference (11) p. 295)

$$a = h_o - T_d (s - s_d) - h_d \qquad (8)$$

where s represents the entropy of unit mass. The temperature of the dead state we will take as $530°R$ (room temperature). The pressure of the dead state will not be required. In the experiments now to be analyzed the stagnation temperatures of both fluids remain at $530°R$ throughout. Hence h_o and h_d both remain constant and the increase in availability as fluid passes from some state i to another state j is $a_j - a_i = T_d(s_i - s_j)$.

If we multiply this quantity by the appropriate mass rate of flow $\dot{m}$, we obtain the rate at which the available energy of the stream increases because of the process i, j. This rate is

$$\dot{m}(a_j - a_i) = \dot{m}T_d(s_i - s_j). \qquad (9)$$

All changes in the available energy of the driving stream are decreases. For the driven stream there is an increase in available energy as the useful work of compression is done on it, but a decrease when no such work is being done. An efficiency η_a based on available energy changes, rather than on isentropic enthalpy changes, can be computed. For the present case where no stagnation enthalpy changes are involved

$$\eta_a = \omega \; \frac{(s_8)_3 - s_3}{s_1 - (s_8)_1} \qquad (10)$$

where $(s_8)_3$ is the entropy per unit mass of unmixed driven fluid at the pressure P_8, and $(s_8)_1$ is the corresponding entropy of driving fluid at the same pressure.

This definition of efficiency is theoretically preferable to that of Eq. (1) and (2) but is not commonly used. Computed values of η_a

for run 45 are given in Table 1, part a, where they may be compared with the corresponding values of η.

The change in entropy of an ideal gas between two states i and j is

$$s_j - s_i = c_p \ln \frac{T_j}{T_i} - R \ln \frac{P_j}{P_i} \tag{11}$$

This equation holds whether or not the gas is in motion, but for a moving gas the local rather than the stagnation variables must be used. Equation (11) permits the desired entropy changes involving states 1, 3, 5, 6, 7, and 8 to be calculated, after which the availability changes are readily obtained. The pressures of all states are known from observation. The temperatures of the stagnation states 1, 3, and 8 are taken to be 530°R.

The temperatures of states 5, 6, and 7 must be calculated. The velocities u_5, u_6, and u_7 have been computed in connection with the momentum-flux balance. The corresponding temperatures are obtained from the energy equation, written in the form

$$T = T_o - \frac{u^2}{2c_p} \tag{12}$$

using the appropriate heat capacity for the stream whose temperature is being calculated.

In calculating entropies and availabilities for the mixed states 7 and 8, the entropy of mixing has been ignored. The temperatures calculated from Eq. (12) are used, together with the observed pressures. A separate calculation is made for each gas even in the mixed states 7 and 8, using the values of R and c_p appropriate to the gas in question. If the entropy of mixing were to be included, the same procedure would be used except that the partial pressure of the appropriate component would be substituted rather than the observed pressure exerted by both components. It is common practice in calculations of efficiency or availability to ignore the fact that the streams are mixed. The investigator says, in effect, "I am indifferent to the fact that the two streams mix; therefore I will compute efficiencies and availabilities in such a way as to ignore the mixing."

The fact that the two streams mix has not been ignored in the computation of any physical process. To do so would of course be improper. For example, in using Eq. (4) to get u_7, or Eq. (12) to compute T_7, the values of R, c_p, and $\dot{m}$ used must refer to the mixture. In this connection it may be noted that in addition to the equalization of velocity, temperature, and pressure during mixing there is in general a flow of heat from one component to the other. This flow of heat also takes place in the diffuser if the driving and driven fluids are different. Stated otherwise, the two components in the diffuser would, if compressed separately from T_7 and P_7 to P_8, have different temperatures, one above, the other below the actual T_8.

The results of calculations of available-energy changes in run 45 are given in Table 1. Part d contains the changes experienced by the driving fluid. The total change is given first, followed by the changes in individual steps, each given as a percentage of the overall change. Table 1, part e, contains similar information for the driven fluid. In Fig. 9a, the results for the driving stream are shown as functions of the outlet pressure P_8. The actual changes, rather than the percentages of the total change, are plotted. No corresponding graph for the driven fluid is given, but the overall increase in available energy of the driven fluid is necessarily equal to the useful work done by the driving fluid, which is shown in Fig. 9a.

Calculations of changes in available energy similar to those just described were made for a second run (run 19, air:air), and the results are shown in Fig. 9b.

In studying Fig. 9 we first note that the useful work is, unfortunately, quite small in comparison to the losses. The deceleration loss is not large except for very low values of P_8 in run 45. The loss in this region is large only because P_8 is being maintained at so low a value that the diffuser has no chance to operate normally. Instead of containing subsonic flow in a rising pressure gradient, the diffuser appears to contain some supersonic flow and a weak shock pattern. In connection with the relatively small deceleration losses, it should be noted that our calculations of momentum-flux balance indicated that our estimates of state 7 might be in error. If the equivalent momentum-flux of state 7 were increased, the losses attributed to deceleration would be increased and those attributed to mixing would be decreased.
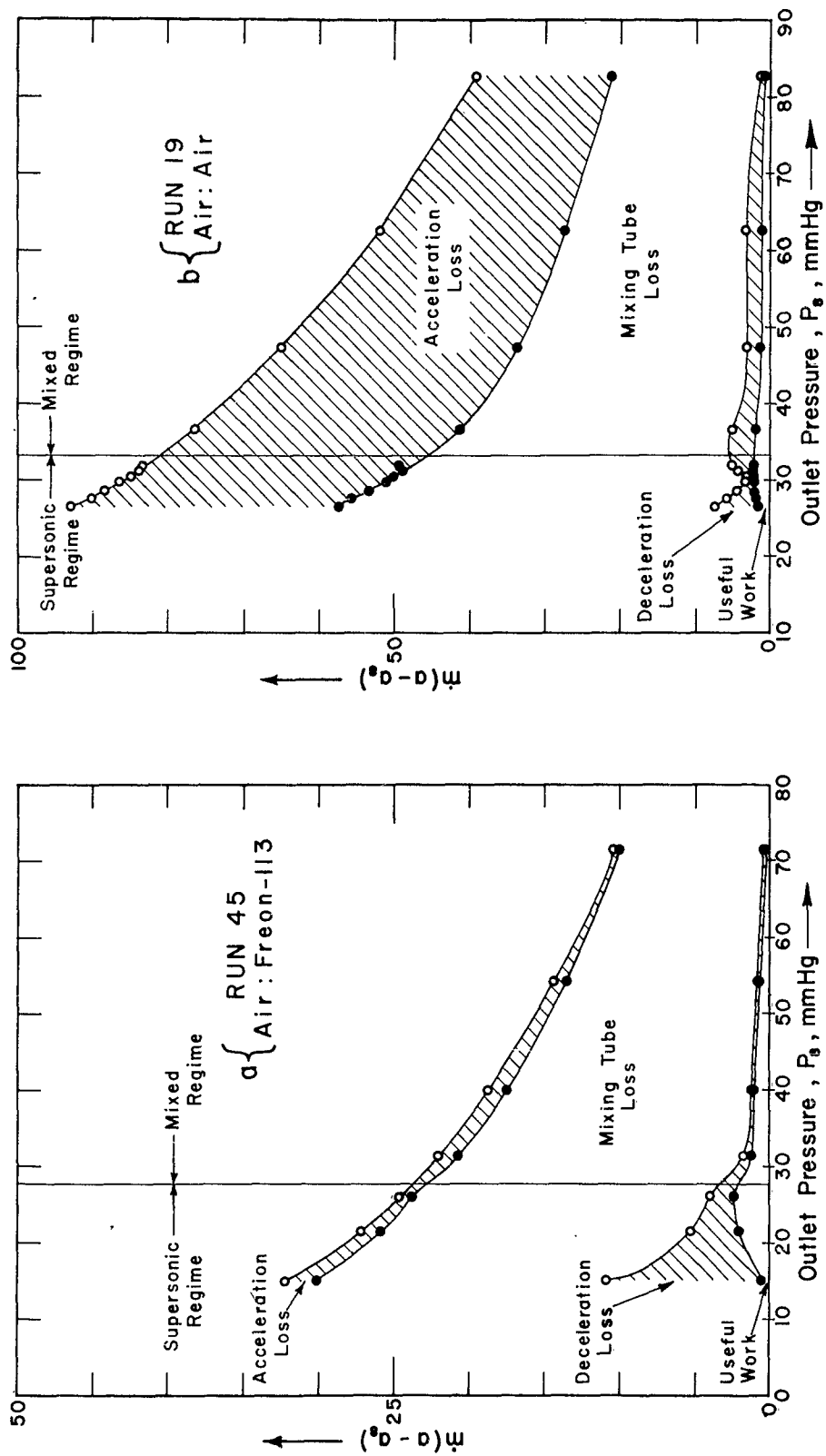
45

Fig. 9. Graph showing how the fall in available energy of the driving stream is accounted for. The upper line shows the total drop. The distance between two curves shows the amount of energy going into a particular drop, or into useful work, as indicated. Note the much greater acceleration loss when the driving fluid is air than when it is Freon-113.

The mixing-tube losses are large, especially in run 45. Part of these losses are associated with friction and with heat conduction due to nonuniformity of static temperatures within a single stream. Over these losses we have little control. Another part of the mixing-tube losses is the mixing loss proper, which has to do with the equalization of pressure, temperature, and velocity between the two streams. This loss resembles a shock loss in that the mixing equations cannot in general be satisfied without an increase in entropy. The mixing loss proper we may hope to exercise some control over, by proper choice of working fluids, velocities, pressures, and possibly other variables.

The driving-fluid acceleration loss is rather small for Freon-113 (run 45) but is much larger for air (run 19). Such a result had been foreshadowed in the calculation of separation, where the deviation from isentropic flow, as specified by the pressure ratio P_{5s}/P_5, was found to be 0.95 for Freon-113, but only 0.53 for air. It is probable that the large acceleration loss shown by run 19 occurs because of the small size of the nozzle. In a larger, or perhaps in a better-designed nozzle, one would expect the percentage losses to be much smaller.

The breakdown of losses confirms what we have known all along: that the largest losses in a jet compressor are associated with the mixing process. Our calculations show that most of the useful work performed in a jet pump is done in the mixing tube, but indicate that a small amount of useful work is done in the diffuser. It may be argued that this situation does not truly exist; that it results from some inaccuracy in the way in which state 7 is calculated. One thing appears certain: heterogeneous entrainment, in which the driving and the driven gases have different molecular weights and different specific heats, offers greater opportunity than self-entrainment for achieving the optimum conditions of mixing.

9. Mixing Pressure and Efficiency

There have been indications (for example reference (12) page 306) that constant-pressure mixing is superior to mixing in which the two streams are at different pressures when they come in contact. The term "constant-pressure mixing" is really somewhat ambiguous. In its strictest sense, such mixing requires that all flow should be at the same constant pressure throughout the mixing tube, a situation that would require a careful choice of mixing-tube shape and a particular entrainment ratio.

The restriction to constant-pressure mixing is often applied to simplify momentum-flux control-volume calculations, and for this purpose it is necessary to assume constant pressure only in those portions of the mixing tube where the channel is converging or diverging.

The present experiments, which were performed with constant-area mixing, cannot give true constant-pressure mixing. We can, however, determine whether or not the highest efficiencies are obtained when mixing starts at constant pressure, that is, with $P_6/P_5 \doteq 1$. Table 2 contains the values of P_6/P_5 that corresponded to the peak efficiency of every run now being reported. It can be seen that the value of P_6/P_5 at maximum efficiency is only occasionally close to unity.

The behavior of P_6/P_5 in the course of two different runs in which outlet pressure P_8 was varied is shown in Fig. 10. The runs selected are 45 and 19. Values of P_6/P_5 for the first of these will be found in Table 1, part a. As the outlet pressure is raised, there is at first no change or only a small change in P_6/P_5. This is characteristic of the supersonic regime, in which downstream conditions have no effect on upstream conditions. As P_8 is further raised, the transition from the supersonic to the mixed regime occurs. Vertical dividing lines based on the criteria accepted earlier are shown in the figure. The supersonic regime (S) lies to the left of the dividing line and the mixed regime (M) to the right, as indicated for each curve. While the transition is taking place the value of P_6/P_5 rises rapidly, but it levels off at a new, higher value. The arrows in the figure indicate the points at which the maxima in the corresponding efficiency curves occur. There is no arrow in the mixed regime of run 19 because the efficiency in this regime was monotonic; the efficiency steadily fell as P_8 was increased.

When P_6/P_5 remains constant in the supersonic regime it is because P_6 and P_5 individually remain constant. In the mixed regime, both P_6 and P_5 increase with P_8, and a constant ratio results from equal fractional changes in both. In many runs the upper portions of the P_6/P_5 curves were not horizontal as in Fig. 10, but rose to a maximum value of 1.25 or 1.30 and then fell again. In other cases the curves sloped steadily upward throughout the range of P_8 covered.
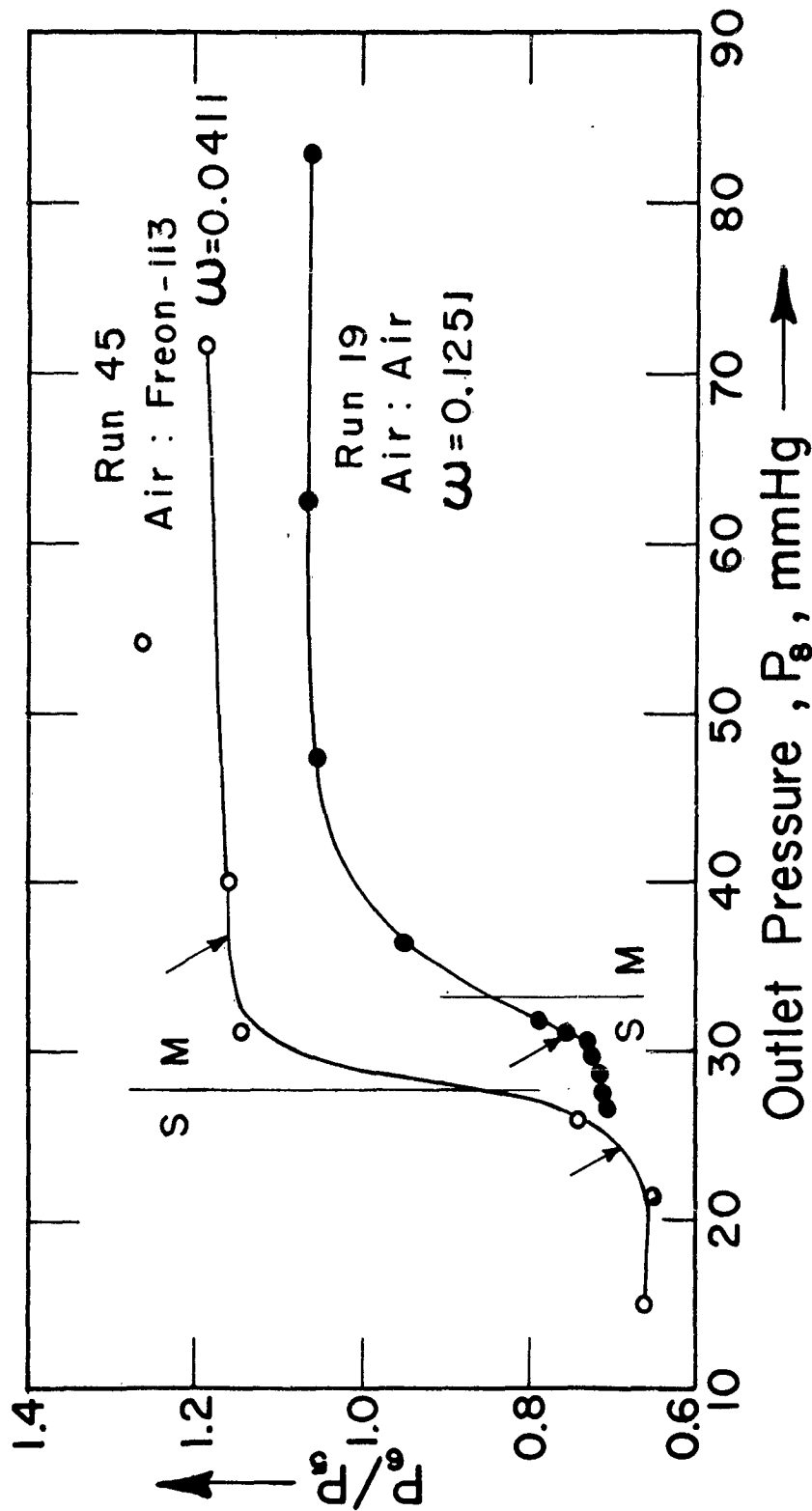
Fig. 10. Mixing-pressure ratio (P_6/P_5) as a function of outlet pressure (P_8), for two selected runs.

If we consider only the point or points of maximum efficiency for each run, we may (from the data in Table 2) plot P_6/P_5 versus entrainment ratio. This has been done in Fig. 11 for the system air:Freon-113 and for the system air:air. The first system has two widely-separated curves: one for the supersonic regime lying well below $P_6/P_5 = 1$ and one for the mixed regime lying above $P_6/P_5 = 1$. Similar curves were found for all systems except air:air.

The air:air system was unique in two ways. First, a few of the supersonic-regime points actually had P_6/P_5 greater than 1. Second, there were two distinct supersonic-regime curves, analogous to the curves S1 and S2 in Fig. 5, and labeled to correspond. The mixed-regime curve for air is quite flat in Fig. 11, and continued to be flat beyond the range of the graph, the last measurement being at $\omega = 0.5319$.

These results show that for the present apparatus the highest efficiencies were not obtained at $P_6/P_5 = 1$. Whether this is true of all constant-area ejectors is not known. Perhaps as the area ratio A_6/A_5 is varied, a condition is reached for which the highest efficiency is obtained with $P_6/P_5 = 1$.

A curve similar to those in Fig. 11 was given in one of our previous publications (Fig. 7 of reference (1)). This curve is for the air:air system but is somewhat different in shape from the air:air curves in Fig. 11. Presumably the difference is due to the difference in geometry of the two apparatuses. The curve in reference (1) reaches $P_6/P_5 = 1.4$, whereas in Fig. 11 the highest value is 1.05. The earlier curve covers a much larger entrainment ratio than the present one. In reference (1) the pressure P_5 was not actually measured, but was calculated from the stagnation pressure P_1 and the nozzle dimensions. An allowance was made for losses, but on the basis of our experience since that time, the allowance was probably low. With greater losses, P_5 would be increased, and the curve of P_6/P_5 in reference (1) would be lowered somewhat.

When reference (1) was published, we considered the ratio $P_6/P_5 = 1.4$ so small as to indicate no danger of separation in the driving-fluid nozzle. On the basis of our experience with the present apparatus we cannot be sure that separation did not occur at the upper end of the curve in Fig. 7 of reference (1).
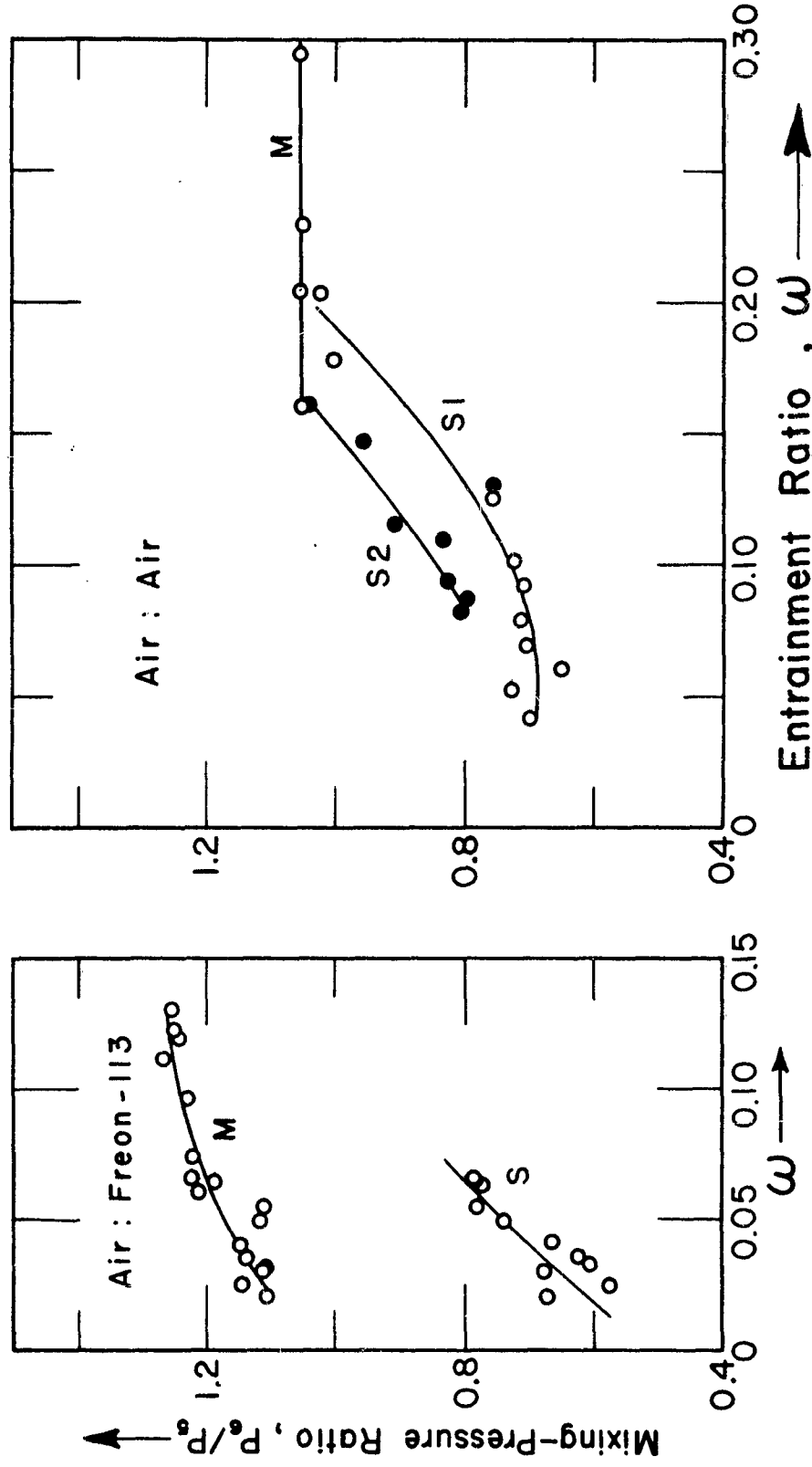
Fig. 11. Mixing pressure ratio at η_{max} versus entrainment ratio, for two selected systems.

10. Some Unexplained Phenomena

There are a few small effects and peculiarities in the data that we have so far not been able to explain by consideration of the various flow patterns described earlier. One of these small effects is shown in Figs. 3 and 4. The general pattern of these curves has been explained by attributing them to the supersonic and mixed regimes. Maxima in the curves may occur in either regime. But a close inspection shows that in addition to a maximum in each regime, many of the curves show other smaller dips or submaxima. These secondary features of the curves exhibit a certain pattern, as may be seen best in the mixed region of Fig. 3.

The existence of dips or irregularities in curves such as those of Fig. 4 was pointed out in reference (1). Their cause has not been definitely established. It may be that they are associated with the shock pattern that must exist as the supersonic flow is dissipated. As operating conditions are changed, the shock pattern probably undergoes a gradual modification brought about by thickening of boundary layers and movement of the planes at which flow separation occurs.

A second unexplained phenomenon is shown in Fig. 5. The supersonic-regime curve for the system He:Freon-113 has a peculiar concave top. Note that this is a somewhat different phenomenon from those discussed above, for here the abscissa is ω rather than P_B and each plotted point in Fig. 5 represents the maximum from an entire run in which P_B was varied. Dips, irregularities, and curves with concave tops are of some importance in jet-compressor design. For example, we estimate that the supersonic-regime curve for He:Freon-113 in Fig. 5 would have risen to $\eta_{max} = 0.15$ if it had been shaped like the adjacent supersonic curve for air:Freon-113. The highest observed point on the concave curve is $\eta_{max} = 0.1254$.

The third and last of the unexplained phenomena is the most obscure of all. For it we refer again to Fig. 5, this time to the curve representing the supersonic regime of the system air:air. This regime has two branches, labeled S1 and S2. An unusually large number of runs were made, to learn more about the curves S1 and S2. A given entrainment ratio ω would give a point lying on one curve, but when ω was changed by even a small amount, a point on the other curve would result. After a large number of runs, it was quite clear that we were not being confused by experimental errors, but that there were in fact two supersonic-regime curves.

Confirmation that the curves S1 and S2 are separate and distinct may be seen in Fig. 11. Here again there are separate curves labeled S1 and S2. But the curves in Fig. 11 depend on P_5 and P_6, whereas those in Fig. 5 depend on P_1, P_3, and P_8. Errors in pressure measurement could hardly affect Figs. 5 and 11 similarly, and yet with only one exception (point 88.4) the points lying on S1 in Fig. 5 also lie on S1 in Fig. 11. An equivalent statement is true for the curves S2.

11. Efficiency at Constant Outlet Pressure

Many investigators have studied the performance of the jet pump under conditions of constant outlet pressure P_8. This is convenient when for example the pump exhausts to the atmosphere. In such investigations the inlet pressure of the driving fluid (P_1) is usually held constant, and the inlet pressure of the driven fluid (P_3) is varied. This causes a variation in the mass rate of flow of driven fluid and hence in the entrainment ratio ω.

Selected Data from this Research. Our own apparatus was not so well adapted to operation at constant P_8 as at constant ω. However, it is possible by reading values from a series of curves, such as those in Fig. 3 and Fig. 4, to obtain data equivalent to a run at constant P_8 and varying ω and P_3. Figure 12 shows results found in this way for the system air:Freon-113. Efficiency is plotted versus entrainment ratio, for three selected values of P_1/P_8. The curve for the highest value of P_1/P_8 (6.5) rises steeply with increasing ω to a maximum value of 0.1135 and then drops abruptly to values less than half of this. All the high-efficiency points prior to the sudden drop correspond to the supersonic regime. All the points after the drop correspond to the mixed regime. A considerable amount of extrapolation was involved in getting the section of the curve corresponding to the mixed regime. This section of the curve is dashed to indicate its lower accuracy.

At the lowest value of P_1/P_8, which was 4.5, all plotted points come from the mixed regime. The curve rises smoothly to a maximum efficiency of 0.0847 at an entrainment ratio of 0.0739. At the intermediate value of P_1/P_8, which was 5.5, the curve is intermediate in character between the two extreme curves. The points of this curve at low values of ω lie in the supersonic regime and those at high values lie in the mixed regime. It is difficult to pick a precise dividing line between the two regimes because the transition from one to the other is continuous, but as a rough value we may take $\omega = 0.045$.

<u>Selected Data from Fabri and Siestrunck</u>. Data from Fabri and
Siestrunck (3) permit the calculation of efficiencies. Their Fig. 7
gives the entrainment ratio as a function of P_3/P_8, for four constant
values of P_1/P_8. The curve for $P_1/P_8 = 5.5$ was selected, and the
abscissa and ordinate of each plotted point were read from the graph.
These data were used to compute η, and a graph of η versus ω (for
$P_1/P_8 = 5.5$) was plotted.

The curve was parabolic, roughly similar to the curve in our
Fig. 12 for $P_1/P_8 = 4.5$. The maximum efficiency of 0.126 occurred
at $\omega = 0.23$. The data came from the supersonic and saturated super-
sonic regimes of flow. There was no sharp drop in the curve similar
to those appearing in two of the curves of Fig. 12. Presumably the
sharp drop occurs only when there is a transition from the supersonic
to the mixed regime, a situation that did not exist in the data taken
from Fabri and Siestrunck.

12. <u>Test of a Method for Calculating the Supersonic Regime</u>

Fabri and Siestrunck (3) have developed methods for calculating
a number of different regimes of flow in constant-area mixing. We
will confine our attention to their method for calculating the super-
sonic regime. This is probably the most important of the various
regimes in jet-compressor applications. The assumptions made by these
authors permit us to go beyond the usual calculation, and to predict
the mass rate of flow of driven fluid as a function of its initial
stagnation pressure. The state of the driving stream at entrance to
the mixing tube is given. The state of the mixed stream at the outlet
need not be known, except that it must be such as to permit the super-
sonic regime to exist.

Using their assumptions, Fabri and Siestrunck have calculated and
plotted curves that agree well with their experimental points. We
think it important to test their methods by applying them to other ex-
perimental data taken in apparatuses of different geometry, for if the
methods of predicting the behavior of ejectors can be shown to be
generally applicable they will be very useful.

The method of Fabri and Siestrunck for calculating the supersonic
regime is based on the assumption that the driven stream may be con-
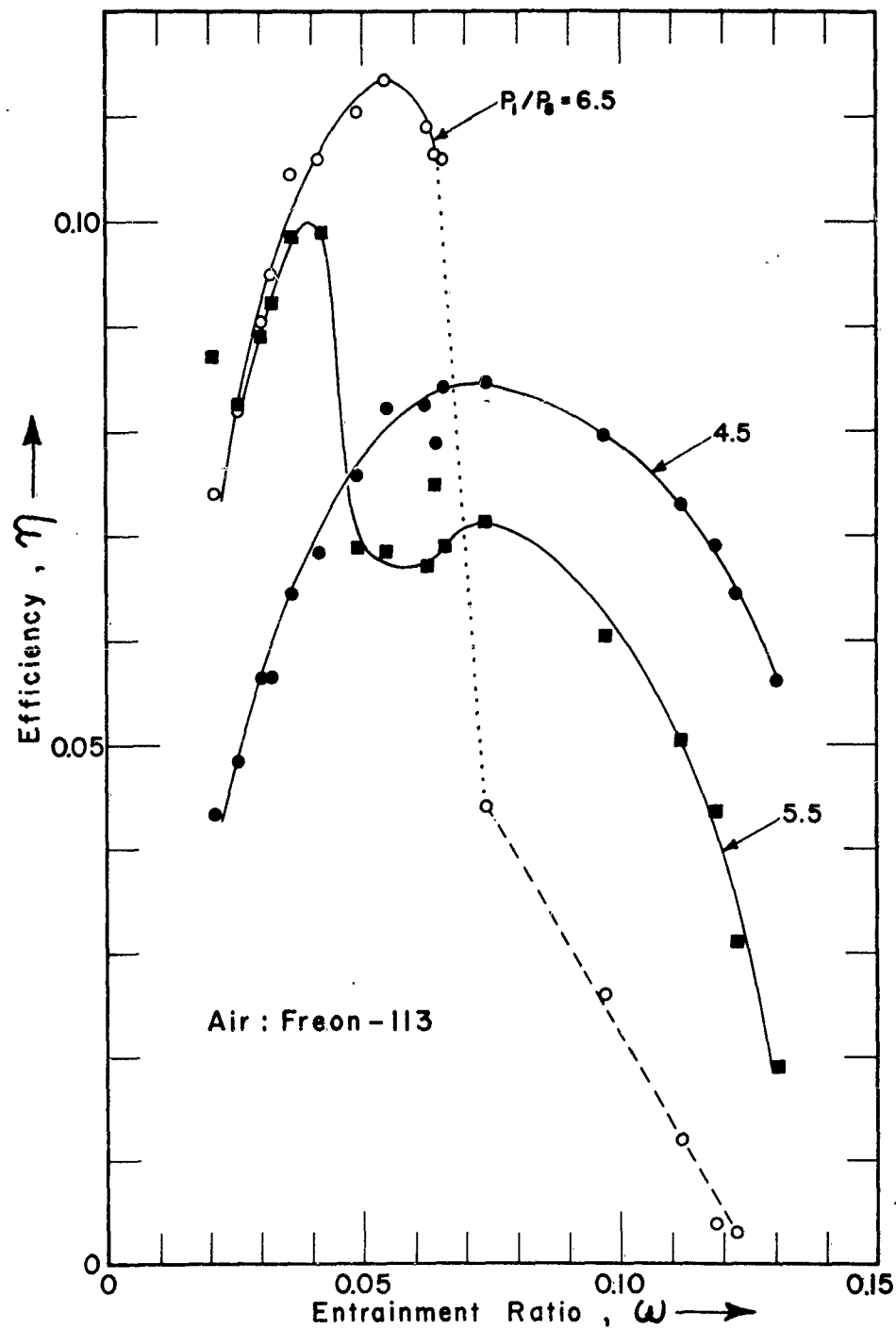sidered as expanding isentropically within the mixing tube until it

Fig. 12. Efficiency as a function of entrainment ratio at constant outlet pressure. Points were obtained by reading values from graphs such as Fig. 3.

becomes sonic. The supersonic driving stream also is considered to expand isentropically as it flows beside the driven stream. Energy is considered to be conserved in each stream separately. The momentum flux of the two streams at the plane where the driven stream becomes sonic is equated to the momentum flux of the input states 5 and 6 (see Fig. 1). The equation permits the mass rate of flow of driven fluid and the pressures in the driven stream at the various points of interest to be found.

With the assumptions outlined above it is not possible to assume that the two isentropic streams have equal pressures at the cross section where the driven stream becomes sonic, and hence the calculated conditions cannot in general actually exist within the mixing tube. It is still possible, however, for the momentum-flux calculated from this admittedly incorrect model to be a good approximation to the actual momentum flux in the mixing tube.

For a test of the method outlined above with our data, we chose the system air:Freon-113, and used the point of lowest P_8 in each run, except that those runs in which the supersonic regime did not appear were excluded. If the supersonic regime appears at all, it is most likely to appear at the lowest value of P_8 attained. The selected points are plotted in Fig. 13, which shows entrainment ratio ω as a function of P_3, the initial pressure of the driven fluid.

The relation between ω and P_3 was then calculated by the method of Fabri and Siestrunck, using the known dimensions of our apparatus, the known properties of air and Freon-113, and the known flow rate and entrance conditions of the driving stream. The details of the analysis were handled by methods differing somewhat from those given by Fabri and Siestrunck. In reference (13) it is shown that the pressure-area terms in the momentum-flux equation can be expressed entirely in terms of M^*, the velocity number of the stream, which is defined as u/c^*. The equation in terms of M^* can be used before the pressures have been determined, thus simplifying the computations. We assigned values to M^*_6 at the beginning and found the corresponding values of P_6 near the end of each calculation.

The calculated results are shown by the upper curve in Fig. 13. The curve, in spite of all the functions from which it is derived, is almost a straight line. Qualitatively it represents the data.
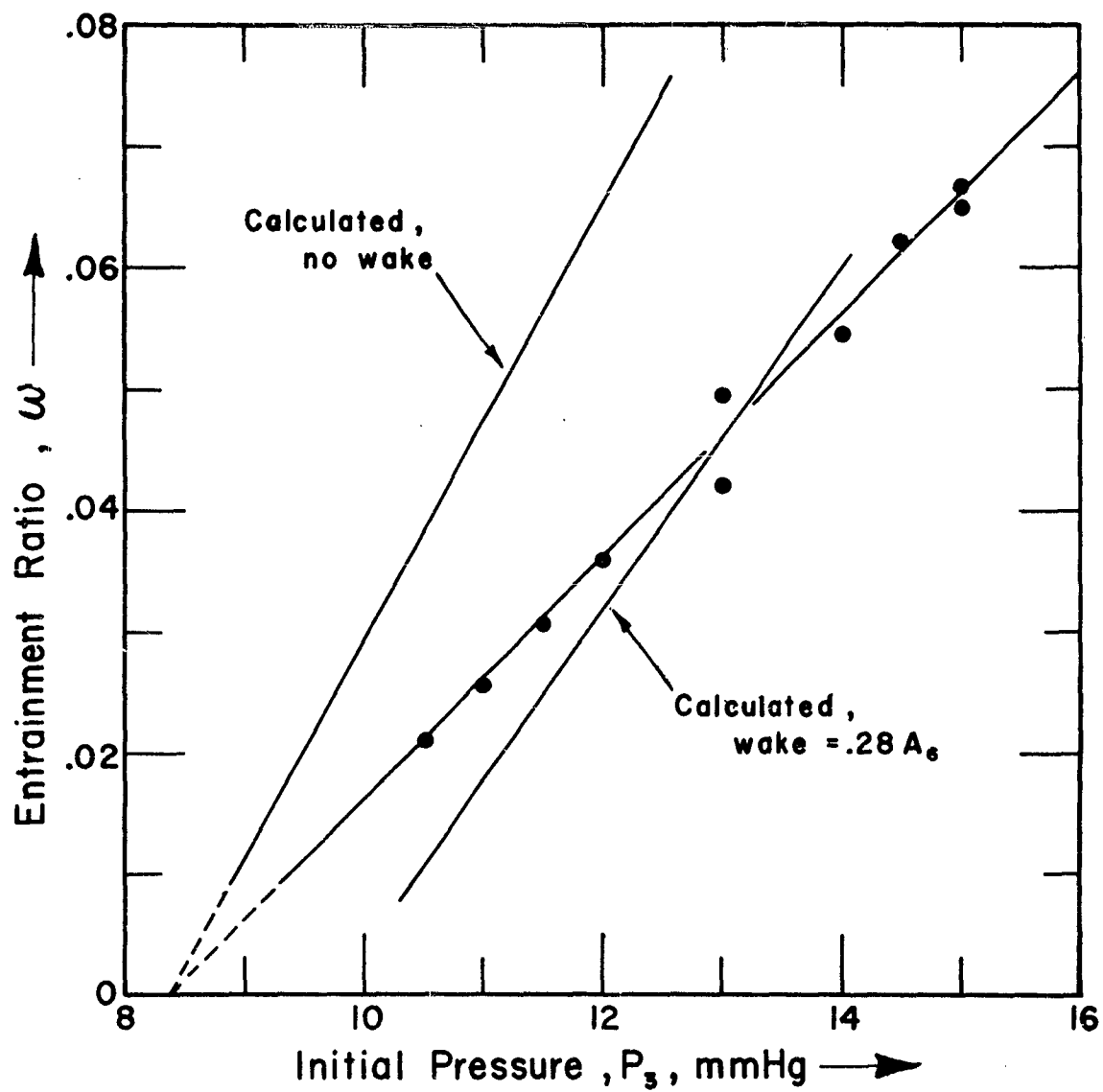
Fig. 13. Entrainment ratio versus P_3 for the system air:Freon-113, in the
supersonic regime. Plotted points are experimental data, curves
are calculated.

The curve is too steep and it gives entrainment ratios that are too high, but nevertheless it is an achievement to be able to calculate such a curve without reference to the experimental data.

An empirical correction was made to the calculated curve by adding the term ΔP (mmHg) $= 45 \, \omega$ to each calculated pressure. This yielded the curve that has been drawn through the points. The value of adding this correction is debatable, however, as long as its magnitude has to be empirically determined.

Fabri and Siestrunck say that it is necessary to take into account a wake of constant width, which they picture as separating the two streams within the mixing chamber. We have tried this, deducting a wake of area $0.28A_6$ from both A_6 and A_7 but leaving A_5 unchanged. (We first deducted half the wake from A_5 and half from A_6, but this led to the impossible situation of a higher stagnation pressure in state 5 than in the original state 1.)

The result of deducting the wake is shown in Fig. 13. The curve based on the assumption of a wake represents the experimental data better than the curve for which no wake was assumed, but the slope is still too great and the wake-curve does not extrapolate to agree with the experimental data at $\omega = 0$, whereas the no-wake-curve extrapolates correctly.

Still another type of wake was tried, in which the wake was of variable width, calculated according to the equation A (wake, in.^{2}) $=$ $0.02439 \, M^*_6$. This gave a line more strongly curved than any of those shown in Fig. 13. This line represented the data better than any of the curves except the one in which the empirical correction $\Delta P = 45 \, \omega$ was used.

It is possible that better fits could be obtained by different assumptions regarding the wake. We ignored the PA-terms contributed by the two ends of the wake, and assume the previous workers did likewise. However, as long as the size of the wake has to be estimated empirically, its use does not greatly increase the usefulness of the theory.

When Fabri and Siestrunck's picture of the supersonic regime is adopted, the equivalent momentum flux in the plane 5,6 (see Fig. 1)

58

is set equal to the equivalent momentum flux at the plane where the driven stream becomes sonic. It is of interest to see if the calculated flux at intermediate planes has the same value. We can calculate the area required by the driven stream as a function of its velocity number, and deduct it from the area of the mixing tube to find the area remaining for the driving stream. If we assume that the driving stream expands isentropically in the area allotted to it, we find that the equivalent momentum-flux equation is satisfied only at the planes where equality was imposed, but not at intermediate planes. The calculated equivalent momentum flux was too large at intermediate planes, for the case we investigated.

The assumption of a wake of suitably varying width would make the flow postulated by Fabri and Siestrunck more plausible. Their picture might also be improved if the generalized choked flow described in reference (6) were assumed, and its equivalent momentum flux used rather than that at the plane where the driven flow becomes sonic.

13. Discussion

The operation of the jet compressor is now partially, but not completely, understood. The immediate cause for each change in flow pattern can generally be identified. For example, we associate the transition from the supersonic to the mixed regime with the penetration of downstream pressure along the walls of the mixing tube so that a supersonic barrier between inlet and outlet no longer exists. We can tell from the data approximately when separation of supersonic flow begins in the driving-fluid nozzle.

Models of flow have been proposed that permit us to calculate the behavior of an ejector from its geometry, from a knowledge of the external states of the streams, and from their thermal properties. These models must in some way take into account the interaction of the two streams after they enter the mixing tube. Our concepts of the flow patterns are in need of further testing and refinement.

Most of the models so far proposed treat the two streams as either completely separate or completely mixed. This may be satisfactory for self-entrainment of fluids having equal stagnation temperatures, but in heterogeneous entrainment the admixture of even a small fraction of the driving stream with the driven stream can cause a substantial change in

the conditions of choking. This will make it difficult to make accurate predictions of when choking will occur.

Our own future plans involve the use of a third apparatus, consisting of a second flat bar for insertion into the assembly shown in Fig. 2. This second flat bar has A_6/A_5 approximately equal to 1, as compared to $A_6/A_5 \doteq 2.04$ in the present apparatus.

14. Acknowledgment

The authors wish to thank Dr. Lois C. K. Carwile for valuable aid in the preparation of this report.

15. References

1. Harold J. Hoge, Suzanne S. Eichacker, and David L. Fiske, "Studies of Jet Compression --1. Apparatus and Methods. Results with Air at Room Temperature," J. Basic Engineering, Trans. Am. Soc. Mech. Engrs. D81 (1959), 426-32.

2. Suzanne S. Eichacker and Harold J. Hoge, "Jet-Compressor Efficiencies as Influenced by the Nature of the Driving and Driven Gases," J. Aerospace Sciences 27 (1960), 636-7.

3. J. Fabri and R. Siestrunck, "Supersonic Air Ejectors," Advances in Applied Mechanics 5 (1958), 1-34.

4. J. Fabri, E. LeGrives, and R. Siestrunck, "Aerodynamic Study of Supersonic Flows," Jahrbuch 1953 der Wissenschaftlichen Gesselschaft für Luftfahrt, F. Vieweg u. Sohn, Braunschweig (1954) p. 106-10.

5. Anthony Fortini, "Performance Investigation of a Nonpumping Rocket-Ejector System for Altitude Simulation," Natl. Aero. Space Admin. Tech. Note D-257 (Dec. 1959), 33 p.

6. H. Pearson, J. B. Holliday, and S. F. Smith, "A Theory of the Cylindrical Ejector Supersonic Propelling Nozzle," J. Roy. Aero. Soc. 62 (1958) 746-51.

7. Joseph H. Keenan and Joseph Kaye, <u>Gas Tables</u>, John Wiley & Sons, New York (1948), 238 p.

8. Martin Summerfield, Charles R. Foster, and Walter C. Swan, "Flow Separation in Overexpanded Supersonic Exhaust Nozzles," Jet Propulsion 24 (1954), 319-21.

9. E. I. du Pont de Nemours & Co., Wilmington 98, Delaware, Freon Technical Bulletin B-2 (copyright 1957), 11 p.

10. William H. McAdams, Heat Transmission, McGraw Hill Book Co., New York, 3d ed. (1954). [Chart on p. 156 was used.]

11. Joseph H. Keenan, Thermodynamics, John Wiley & Sons, New York (1941).

12. J. H. Keenan, E. P. Neumann, and F. Lustwerk, "An Investigation of Ejector Design by Analysis and Experiment," J. Appl. Mech. 17, Trans ASME 72 (1950), 299-309.

13. Harold J. Hoge, "On the Theory of Mixing of Fluid Streams," Quartermaster Research and Engineering Center, Tech. Rept. PR-2 (Feb. 1959), 58 p.

DISTRIBUTION LIST

Copies

2	Commanding General, U. S. Army Materiel Command, Washington 25, D. C.
2	Commanding General, Hqs., U. S. Army Electronics Command, Fort Monmouth, N. J.
2	Commanding General, Hqs., U.S. Army Missile Command, Redstone Arsenal, Huntsville, Alabama
2	Commanding General, Hqs., U.S. Army Mobility Command, 28251 Van Dyke Avenue, Center Line, Michigan
2	Commanding General, Hqs., U. S. Army Munitions Command, Picatinny Arsenal, Dover, New Jersey
2	Commanding General, Hqs., U. S. Army Supply and Maintenance Command, Washington 25, D. C.
2	Commanding General, U. S. Army Test and Evaluation Command, Aberdeen Proving Ground, Md.
2	Commanding General, Hqs., U. S. Army Weapons Command, Rock Island Arsenal, Rock Island, Illinois
1	Commanding Officer, U.S. Army Combat Developments Command, Fort Belvoir, Virginia
1	Commandant, U.S. Marine Corps, Washington 25, D. C.
10	Commander, Armed Services Technical Information Agency, Arlington Hall Station, Arlington 12, Virginia
1	Commanding General, U.S. Army Combined Arms Group, Fort Leavenworth, Kansas
1	Commandant, U.S. Army War College, Attn: Dir., Doctrine and Studies Div., Carlisle Barracks, Pa.
1	Commanding Officer, U.S. Army Combat Service Support Group, Ft. Lee, Virginia
1	Commanding Officer, U.S. Army Office of Spec. Weapons Development, Ft. Bliss, Texas
1	Commanding General, U.S. Army Combat Developments Experimentation Center, Ft. Ord, California
1	Commanding General, U.S. Continental Army Command, Ft. Monroe, Va.
1	President, U.S. Army Artillery Bd., Ft. Sill, Okla.
1	President, U.S. Army Armor Bd., Ft. Knox, Ky.
1	President, U. S. Army Infantry Bd., Ft. Benning, Ga.
1	President, U.S. Army Air Defense Bd., Ft. Bliss, Texas
1	President, U. S. Army Airborne and Special Warfare Bd., Ft. Bragg, N.C.
1	President, U.S. Army Aviation Bd., Ft. Rucker, Ala.
1	Commanding Officer, U.S. Army Arctic Test Bd., Ft. Greely, Alaska
1	Commandant, U. S. Army Command and General Staff College, Attn: Archives, Ft. Leavenworth, Kansas
1	United States Army Research Office, Box CM, Duke Station, Durham, N.C.
1	Director, U.S. Army Engineer Research and Development Labs., Attn: Technical Document Center, Fort Belvoir, Va.

Copies

2	QM Liaison Officer, ASDL-8, Wright-Patterson AFB, Ohio
2	Director, U.S. Army Ballistic Research Laboratory, Aberdeen Proving Ground, Maryland
1	Director, U. S. Army Materials Research Agency, Watertown Arsenal, Watertown 72, Mass.
1	Commanding General, U.S. Army Nuclear Defense Laboratory, Army Chemical Center, Maryland
2	Commanding General, U.S. Army CBR Agency, Army Chemical Center, Maryland
1	Headquarters, U. S. Air Force, DCS/RT, Washington 25, D. C.
1	Chief, Life Sciences Group, Directorate of Research, DCS/Research and Technology, Headquarters, USAF, Washington 25, D. C.
1	Headquarters, Air Materiel Command, Attn: Tech Library, Wright Patterson AF Base, Ohio
1	Headquarters, Strategic Air Command, Offutt Air Force Base, Nebraska
1	Director, U.S. Naval Research Laboratory, Attn: Code 6140, Washington 25, D. C.
1	Director, Biological Sciences Div., Office of Naval Research, Dept. of the Navy, Washington 25, D. C.
1	Chief, Bureau of Naval Weapons, Dept. of the Navy, Washington 25, D.C.
1	Chief, Bureau of Ships, Code 362B, Dept. of the Navy, Washington 25, D. C.
1	Director, Special Projects, Dept. of the Navy, Attn: SP-272, Wash. 25, D.C.
1	Commander, U.S. Naval Ordnance Test Station, Attn: Code 12, China Lake, California
2	Director, Material Laboratory, New York Naval Shipyard, Attn: Library, Bldg. 291, Code 911B, Brooklyn 1, N. Y.
2	U.S. Atomic Energy Commission, Technical Reports Library, Washington 25, D.C.
2	U.S. Atomic Energy Commission, Office of Tech. Information, P.O. Box 62, Oak Ridge, Tennessee
2	Commanding General, Defense Supply Agency, Defense Clothing & Textile Supply Center, 2800 S. 20th St., Philadelphia, Pa.
1	National Research Council, 2101 Constitution Ave., Washington, D. C.
2	Gift and Exchange Division, Library of Congress, Washington 25, D. C.
1	U. S. Department of Commerce, Weather Bureau Library, Washington, D. C.
1	U. S. Department of Agriculture Library, Washington 25, D. C.
1	Commandant, Industrial College of the Armed Forces, Ft. McNair, Washington 25, D. C.
1	Commanding Officer, U.S. Army Signal Research and Development Lab., Ft. Monmouth, N. J.
1	Commandant, Air Defense School, Ft. Bliss, Texas
1	Commandant, U.S. Army Armor School, Ft. Knox, Kentucky
1	Commandant, U.S. Army Artillery School, Ft. Sill, Oklahoma
1	Commandant, U. S. Army Aviation School, Ft. Rucker, Alabama
1	Commandant, U. S. Army Infantry School, Ft. Benning, Georgia
1	Commandant, U.S. Army Special Warfare School, Ft. Bragg, N. C.

Copies

1	Commandant, US Army Engineer School, Ft. Belvoir, Virginia
1	Commandant, US Army Transportation School, Ft. Eustis, Virginia
1	Commandant, The QM School, Attn: Library, Ft. Lee, Virginia
1	Commanding Officer, Cold Weather & Mountain Indoctrination School, Ft. Greely, Alaska
1	Director, Marine Corps Landing Force Development Center, Marine Corps School, Quantico, Virginia
1	Library, Arctic Institute of North America, 3458 Redpath Street, Montreal 25, P. Q., Canada
1	Director, Air Crew Equipment Laboratory, Naval Air Material Center, Philadelphia 12, Pa.
16	Advisory Bd. on QM R&E, National Research Council, University of Rhode Island, Kingston, R. I.
1	Commander, AF Gambridge Research Ctr., Air Research & Development Cmd., Laurence G. Hanscom Field, Bedford, Mass. Attn: CRTOTT-2
1	Director, Air University Library, Attn: 7575, Maxwell AFB, Alabama
1	The Army Library, Pentagon Bldg., Washington 25, D. C.
1	National Research Council, 2101 Constitution Ave., Washington, D. C.